AGU PUBLICATIONS

JGR

Journal of Geophysical Research: Oceans

RESEARCH ARTICLE

10.1002/2015JC010865

On the seasonal variations of salinity of the tropical Atlantic mixed layer

I. Camara[1,2], Nicolas Kolodziejczyk[2], Juliette Mignot[1,2,3], Alban Lazar[1,2], and Amadou T. Gaye[1]

[1]LPAO-SF, ESP, UCAD, Dakar, Senegal, [2]LOCEAN Laboratory, Sorbonne Universits (UPMC Université Paris 6), CNRS, IRD, MNHN, Paris, France, [3]Climate and Environmental Physics, Physics Institute, Oeschger Centre of Climate Change Research, University of Bern, Bern, Switzerland

Key Points:
- Weak relative surface salinity seasonal variation in the tropical Atlantic
- Compensation between physical processes entering in the salt budget
- Strong contribution of vertical salinity diffusion

Correspondence to:
I. Camara,
ibrahima1.camara@ucad.edu.sn

Citation:
Camara, I., N. Kolodziejczyk, J. Mignot, A. Lazar, and A. T. Gaye (2015), On the seasonal variations of salinity of the tropical Atlantic mixed layer, *J. Geophys. Res. Oceans*, *120*, 4441–4462, doi:10.1002/2015JC010865.

Received 24 MAR 2015
Accepted 14 MAY 2015
Accepted article online 18 MAY 2015
Published online 19 JUN 2015

Abstract The physical processes controlling the mixed layer salinity (MLS) seasonal budget in the tropical Atlantic Ocean are investigated using a regional configuration of an ocean general circulation model. The analysis reveals that the MLS cycle is generally weak in comparison of individual physical processes entering in the budget because of strong compensation. In evaporative regions, around the surface salinity maxima, the ocean acts to freshen the mixed layer against the action of evaporation. Poleward of the southern SSS maxima, the freshening is ensured by geostrophic advection, the vertical salinity diffusion and, during winter, a dominant contribution of the convective entrainment. On the equatorward flanks of the SSS maxima, Ekman transport mainly contributes to supply freshwater from ITCZ regions while vertical salinity diffusion adds on the effect of evaporation. All these terms are phase locked through the effect of the wind. Under the seasonal march of the ITCZ and in coastal areas affected by river (7°S:15°N), the upper ocean freshening by precipitations and/or runoff is attenuated by vertical salinity diffusion. In the eastern equatorial regions, seasonal cycle of wind forced surface currents advect freshwaters, which are mixed with subsurface saline water because of the strong vertical turbulent diffusion. In all these regions, the vertical diffusion presents an important contribution to the MLS budget by providing, in general, an upwelling flux of salinity. It is generally due to vertical salinity gradient and mixing due to winds. Furthermore, in the equator where the vertical shear, associated to surface horizontal currents, is developed, the diffusion depends also on the sheared flow stability.

1. Introduction

In the climate system, ocean and atmosphere interact by exchanging momentum, heat, and freshwater. In the ocean, these exchanges take place in the upper mixed layer. As its name indicates, this layer is well mixed and thus roughly vertically uniform in temperature and salinity. Although temperature generally dominates the density changes in tropical oceans, both temperature and salinity can locally control the stratification, hence the mixed layer depth (MLD).

The tropical Atlantic is characterized by very strong river discharges. The Amazon and the Congo rivers in particular account by themselves for almost 20% of the global amount of rivers discharges. Added to intense precipitations under the intertropical convergence zone, this makes the tropical Atlantic an area of intense spatial heterogeneities of the sea surface salinity (SSS) with potentially important temporal variations. As a result, in several areas of this oceanic basin, the sharp vertical salinity gradient in the upper ocean can limit the depth of the mixed layer. In this case, the isothermal layer found below the mixed layer is called a barrier layer, as it prevents exchanges between the warm mixed layer and the cold ocean interior [*Lukas and Lindstrom*, 1991; *Godfrey and Lindstrom*, 1989]. In the tropical Atlantic, barrier layers among the thickest of the world are found [e.g., *Mignot et al*., 2012], with possibly a strong impact on the oceanic and atmospheric circulations [*Breugem et al*., 2008; *Balaguru et al*., 2012]. More generally, by modifying air-sea interactions, the barrier layers can have important climatic effects [e.g., *Masson et al*., 2005; *Foltz and McPhaden*, 2009; *Grodsky et al*., 2012; *Balaguru et al*., 2012].

Salinity is also an important parameter for the formation and the tracking of water masses [e.g., *Kolodziejczyk et al*., 2014a; *Kolodziejczyk and Gaillard*, 2013, 2012; *Sasaki et al*., 2010; *Yeager and Large*, 2007; *Schneider*, 2000] through its effect on spiciness [e.g., *Jackett and McDougall*, 1985]. Subtropical and tropical water

masses formed thanks to SSS anomalies can be traced along the subsurface currents and reemerge where they could have again major climatic impacts [e.g., *Qu et al*., 2013, 2011; *Langehaug et al*., 2012; *Mignot et al*., 2009; *Laurian et al*., 2009, 2006; *Lazar et al*., 2001].

Finally, several authors have also suggested that the sea surface salinity (SSS) could be used as a rain gauge to assess the global hydrological cycle [e.g., *Bingham et al*., 2012; *Durack et al*., 2012; *Terray et al*., 2012; *Yu*, 2011]. Using World Ocean Atlas 2005 (WOA05) data, *Yu* [2011] investigated the relationship between the mixed layer salinity (MLS) and the ocean water cycle at the global scale. She found that the precipitations mainly control the MLS seasonality in the tropical convergence zones and in the western North Pacific featuring heavy rainfall, while evaporation dominates the subtropical regions. However, this MLS atmospheric forcing is generally modulated in various regions by oceanic processes like horizontal advection by the surface currents and vertical mixing with the subsurface [*Akhil et al*., 2014; *Kolodziejczyk et al*., 2014b; *Hasson et al*., 2013a, 2013b; *Kolodziejczyk and Gaillard*, 2013; *Yu*, 2011]. Documenting the processes that govern the MLS variability is thus crucial to better understand the air-sea freshwater exchanges [*Yu*, 2011]. They are, however, still poorly documented in the tropical Atlantic.

After the pioneering work of *Dessier and Donguy* [1994], *Reverdin et al*. [1997] found that the observed SSS variability is particularly strong in the western tropical North Atlantic and in eastern Gulf of Guinea. Using recent observations of Soil Moisture-Ocean Salinity (SMOS), *Tzortzi et al*. [2013] showed the dominant role of advection and vertical mixing to explain the seasonal cycle of SSS in the eastern tropical Atlantic, where the equatorial cold tongue develops between May and August [*Caniaux et al*., 2011; *Mitchell and Wallace*, 1992]. Based on in situ observations mainly from Argo floats, *Da-Allada et al*. [2013] also found that vertical processes play a major role in the seasonal to interannual mixed layer salinity budget in the Gulf of Guinea (hereafter GG). *Foltz and McPhaden* [2008] used a combination of satellite products, in situ observations, and reanalysis to examine the seasonal MLS balance in the north tropical Atlantic. They found that mechanisms contributing to the salinity balance vary from one region to another. While horizontal advection controls the seasonal cycle of MLS west of 50°W in the northern tropical basin, precipitation is the dominant term south of 14°N. However, these observational studies are limited by data availability and these authors could not compute all terms of the MLS balance, in particular, the vertical mixing and entrainment terms, which were found to be important for the MLS budget in other regions.

These limitations can be partly overcome using oceanic models. *Qu et al*. [2013, 2011], using the Estimating the Circulation and Climate of the Ocean (ECCO) model, investigated the seasonal cycle of the SSS in the northern subtropical Atlantic maximum salinity region. They found weak MLS variations at seasonal time scales, explained by strong evaporation which is compensated by a strong oceanic advection and vertical entrainment of freshwater flux. Recently, *Berger et al*. [2014] and *Da-Allada et al*. [2014] used an ocean general circulation model (OGCM) to investigate the SSS variations in the Gulf of Guinea region. They could quantify the important contribution of the vertical mixing in these regions. It is now needed to expand such quantification to other regions of the tropical Atlantic.

Here we use a regional configuration of the NEMO-OPA OGCM in the tropical Atlantic to quantify the oceanic and atmospheric physicals processes governing the MLS seasonal cycle throughout the whole tropical Atlantic. This study aims at revisiting the MLS budget in the tropical Atlantic with a model simulation, especially by deepening our understanding of the role of processes which cannot be quantified explicitly from data only, namely vertical mixing. This study also focuses on a larger region than previous ones, thereby aiming at providing a general view of the seasonal cycle of the MLS in the tropical Atlantic, identifying dominant processes and possibly similarities among subbasins. The model and validation data are presented in section 2. In section 3, the results are presented, first model validation and mean state, second for regions characterized by the dominant influence of evaporation, third for regions strongly influenced by precipitation, and finally for regions were ocean dynamics play the central role. Summary and discussions are presented in section 4.

2. Model and Data

2.1. Model Description

This study is based on the OGCM NEMO-OPA [*Madec*, 2008]. NEMO-OPA solves the primitive equations on an Arakawa C grid, with a second-order finite difference scheme, assuming the Boussinesq and hydrostatic

approximations, the incompressibility hypothesis, and free surface formulation [*Roullet and Madec*, 2000]. The density is computed from potential temperature and salinity, and pressure, using the *Jackett and McDougall* [1995] equation of state. The horizontal mesh is based on a 0.25° × 0.25° Mercator grid. Realistic bottom topography and coastline are derived from ETOPO2. The maximum depth of 5000 m is spanned by 46 z-level ranging from 5 m thickness in the upper 30 and 10 m thickness around 100 m depth. Vertical mixing of momentum and tracers are computed using a second-order turbulence kinetic energy (hereafter TKE) closure model described in *Madec* [2008]. The ocean model is run with a time step of 1440 s. We use here a new regional configuration of the tropical Atlantic, named ATLTROP025. The grid has been limited to 30°N and 30°S. Ocean boundary conditions are taken from the output of a global 1/4° simulation part of the DRAKKAR hierarchy of global configurations [*Molines et al*., 2007] and detailed in *Brodeau et al*. [2010]. Surface boundary forcing is ensured by bulk formulas developed by *Large et al*. [1997]. Input surface variables needed to estimate air-sea fluxes are wind speed, air temperature, and humidity at 10 m, shortwave and longwave radiations and precipitation. In the present study, they are taken from the climatological seasonal mean of the 6 hourly global DRAKKAR forcing set 4 (hereafter DFS4) [*Brodeau et al*., 2010] computed over the years 1988–2000. Monthly means outputs are used for the purpose of the present study.

2.2. Mixed Layer Salt Budget

In order to understand the processes responsible for the seasonal variations of the salinity, we use a decomposition of MLS budget. This approach has been used in several studies based on observations [e.g., *Da-Allada et al*., 2013; *Kolodziejczyk and Gaillard*, 2013; *Wade et al*., 2011; *Foltz and McPhaden*, 2008] and models [e.g., *Hasson et al*., 2013b; *Qu et al*., 2011]. Following *Vialard and Delecluse* [1998] who evaluated the mixed layer temperature budget, the mixed layer salinity variations can be decomposed as follows, for each horizontal grid point:

$$\partial_t MLS = \overbrace{-\frac{1}{h}\int_{-h}^{0} u\partial_x S dz - \frac{1}{h}\int_{-h}^{0} v\partial_y S dz - \frac{1}{h}\int_{-h}^{0} D_l(S)}^{\text{OCEHOR}} \underbrace{-\frac{1}{h}(MLS - S_h)(w_h - \partial_t h) - \frac{1}{h}[k_z \partial_z S]_h}_{\text{OCEVER}} + \overbrace{\frac{(E-P-R)}{h} MLS}^{\text{FWF}} \quad (1)$$

where S is the salinity, depending on the vertical level; u, v, and w stand for the current in the zonal, the meridional, and vertical direction, respectively, also defined at each model's vertical level. S_h is the salinity at the base of the mixed layer; k_z is the vertical diffusion coefficient; D_l is the horizontal diffusion operator; and h is the depth of the mixed layer, named MLD above. It is computed using a density criterion: it corresponds to the depth at which the density is equal to the sea surface density plus 0.01 kg m^{-3}. Such a small criterion allows the MLS to be a reasonable proxy for the SSS as shown for the temperature by *de Boyer Montégut et al*. [2004].

As explained in example in *Griffies et al*. [2009], forced ocean simulation additionally require an unphysical surface salinity restoring term, in order to prevent uncontrolled drifts in salinity as a response to inaccurate precipitations. Following *Brodeau et al*. [2010], we use a rather strong salinity restoring to *Levitus et al*. [1998] climatology, corresponding to a relaxation time scale of 33 days for the first model level (10 m).

All the terms shown in equation (1) are computed online by the model. The net fresh water fluxes contribution to the MLS budget appears in the last term of the budget, and it is named FWF in the following and is constituted by evaporation (E), precipitation (P), runoff (R), and also the restoring term. All other terms correspond to the net oceanic contribution, noted OCE in the following. The latter can be decomposed into a horizontal (OCEHOR) and a vertical (OCEVER) components. OCEHOR comprises the first two terms in the right-hand side of the equation, that is the horizontal advection (ADVHOR) and the horizontal diffusion (third term). The overall effect of underlying water on the surface is represented by the OCEVER component, which includes the vertical diffusion $-\frac{1}{h}[k_z\partial_z S]_h$ and the so-called other vertical processes (hereafter OVP). The OVP is the sum of vertical advection $-\frac{1}{h}(MLS - S_h)w_h$ and the entrainment $-\frac{1}{h}(MLS - S_h)\partial_t h$. The latter is computed as a residue therefore it may also contain small numerical errors. In the following, special focus

on the physics underlying the vertical diffusion will be made. This term is a function of the MLD, the vertical salinity gradient, and of the vertical coefficient diffusion. The latter is parameterized in the model using the TKE scheme. In this scheme, the diffusion coefficient depends itself on the stratification and the vertical shear, the winds, and the buoyancy. It is thus difficult to interpret the variations of the vertical diffusion physically. Nevertheless, in the TKE scheme, energy available for the diffusion is produced by the momentum shear and destroyed by stratification. Thus, we will also use the nondimensional Richardson number (hereafter *Ri*; $Ri = \frac{N^2}{(\partial_z u)^2 + (\partial_z v)2}$ where N is the Brunt-Väisälä frequency) to compare the relative contribution of these effects. $Ri < 1/4$ is the necessary condition of Kelvin-Helmholtz instability triggering. In the following, we name MLS tendency the time evolution of the MLS, as represented by the left-hand side term of equation (1). This term is also given as a model output.

2.3. Data

When possible, the model results are validated against observational data sets. First, the SSS analysis developed by *Reverdin et al*. [1997] and extended to 2009 was used to validate the modeled MLS. In this analysis, the monthly SSS fields were computed from a variety of data sources, mostly underway collection on research vessels and voluntary observing ships (VOS) through thermosalinograph at a depth 3–5 m (http://www.legos.obs-mip.fr/observations/sss/); PIRATA moorings in the tropical Atlantic (http://www.brest.ird.fr/pirata/), CARIOCA drifters (G. Reverdin, personal communication, 2013), and Argo floats (http://www.coriolis.eu.org/Observing-the-ocean/Observing-system-networks/Argo). These different data sources are gridded using an objective mapping [*Bretherton et al*., 1976] at $1^\circ \times 1^\circ$ spatial resolution.

In order to estimate the error on observed SSS tendencies at seasonal time scales, the monthly SSS error given by optimal interpolated SSS observational field is used [*Reverdin et al*., 1997]. Then errors in SSS tendency were propagated [*Foltz and McPhaden*, 2008] as follows: $e = \frac{\sqrt{(e_{s_{n-1}}^2 + e_{s_{n+1}}^2)}}{\Delta t}$, where e is the SSS error, e_s is the error given by analyzed salinity field $\Delta t = 2$ months.

Mixed layer depth data are taken from the climatology of *de Boyer Montégut et al*. [2004], available monthly on a $2^\circ \times 2^\circ$ grid. It is defined as the depth where the density at 10 m has increased by 0.03 kg m^{-3}. It is estimated from individual temperature and salinity profiles extracted from the National Oceanographic Data Center and from the World Ocean Circulation Experiment database (WOCE Data Products Committee, 2002).

We also use a climatology of near surface currents, at $1^\circ \times 1^\circ$ resolution, derived from satellite-tracked surface drifting buoy observations [*Lumpkin and Garzoli*, 2005].

3. Results

3.1. Overview of the MLS Variability

The simulated annual mean SSS (Figure 1b, colors) is first compared with observations (Figure 1a). The main features of the SSS field are consistently reproduced in the model: the lowest salinity values are found along the northern coast of South America and along the eastern Gulf of Guinea coastal, due to freshwater discharges from rivers (e.g., Amazon, Congo, Niger). Low salinity values are also found between 0°N and 10°N, as a consequence of intense precipitations associated to the intertropical convergence zone (ITCZ). In contrast, SSS maxima are visible in the northern and southern subtropics, where evaporation exceeds precipitation. The SSS maximum in the southern Atlantic is slightly too extended in the model as compared with observations, while the one in the northern hemisphere is slightly shifted southward.

MLS is, however, in fact the relevant variable for our study, rather than SSS. The former is not easily available from observations but the white contours in Figure 1b show that in the model, SSS and MLS are very similar. This gives us confidence in using SSS to validate the model's MLS budget in the rest of this study. The model also reproduces consistently the horizontal surface circulation (Figures 1a and 1b, vectors), in particular, the westward South Equatorial Current (SEC) as well as the North Brazilian Current (NBC) flowing northwestward along the coast. The area of NBC bifurcation (around 7°N/48°W), which is important for the eastern transport of Amazon freshwater, is also well reproduced in the simulation.

The modeled MLD (Figures 1d and 1f, contours) generally agrees with values derived from observations (Figures 1c and 1e, contours). The largest values (70–90 m) are found in the subtropics during local winter, while shallowest MLD values are found along the equator. In the subtropical regions, the model tends to

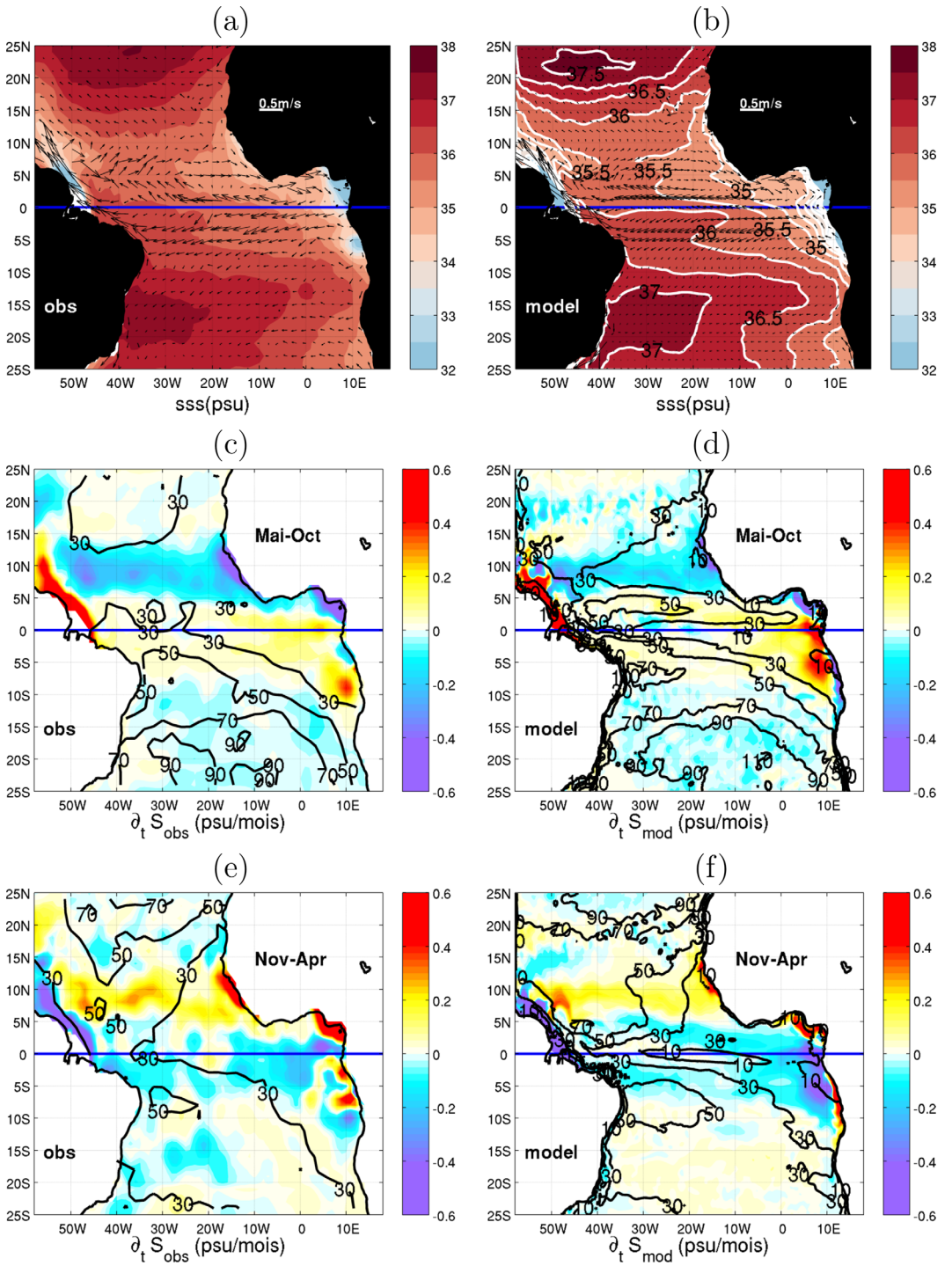

Figure 1. Annual mean SSS (colors, in practical salinity unit (psu)) and surface currents (arrows, in m/s) from (a) observations and (b) the model. White contours in Figure 1b represent the model salinity averaged over the mixed layer depth. (center) May–October mean MLS tendency (colors in psu/mois) and mixed layer depth (contours in m) from (c) observations and (d) the model. (e, f) Same as Figures 1c and 1d for the November–April mean.

overestimate the MLD maximum winter values, consistently with overestimated salinity maximum in the south and shifted location in the north. At the equator, the modeled mixed layer can be thinner than the observed ones. This is likely explained by the 10 m surface reference chosen by *de Boyer Montégut et al.* [2004], which prevents shallower depths to be represented by this product. Differences might also arise from the use of different threshold criteria for the density stratification.

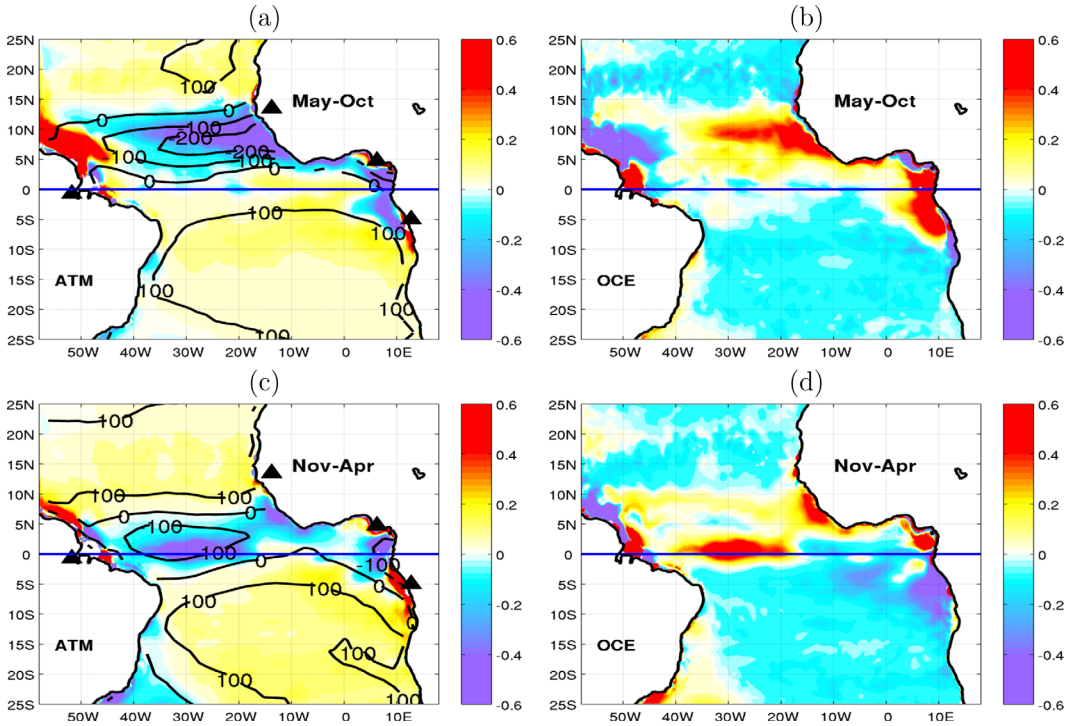

Figure 2. (a) Atmospheric and (b) oceanic contributions to the MLS budget. (c, d) The same as Figures 2a and 2b for November–April mean. Units are in psu/mois. Contours on Figures 2a and 2c are E-P in mm/mois. Triangles in Figures 2a and 2c are rivers positions (Gambia, Niger, Congo, and Amazon).

Finally, as this work focuses on seasonal variations of the MLS, we compare tendencies of the latter during boreal spring-summer (May–October) and boreal fall-winter (November–April) in the model (Figures 1d and 1f, colors) to variations of SSS in the observations over the same seasons (Figures 1c and 1e, colors). The variations of the MLD are relatively weak during each of these seasons. Consequently, the effect of MLD variations on physical processes is reduced. These seasons are also relevant for the ITCZ seasonal path: between May and October, the ITCZ is located around 7°N, inducing intense precipitation at this latitude (Figure 2a, contours). The MLS tendency in the open ocean around this latitude is then dominated by a freshening, while evaporation increases MLS within the equatorial band (Figures 1c and 1d). In November–April, the ITCZ shifts back over the equator, thereby freshening the equatorial band, while salinity increases in the northern tropics (Figures 1e and 1f). The largest seasonal signal of MLS tendency is detected in the coastal regions off northern South American and eastern GG coasts both in the model and the observations. It is explained by the seasonal strong variability of the river discharges. The largest differences between model and observations are also found in these regions (Figures 1c and 1d). This is likely due to sparse observations of the runoff [*Dai and Trenberth*, 2002] as well as difficulties to implement properly this forcing term in the ocean model [*Madec*, 2008].

In order to quantify the respective contribution of atmospheric and oceanic forcing on the MLS tendency, the diagnostic terms are shown separately in Figure 2 for the model only (see section 2 for details). As commented above, the atmospheric contribution appears to be primarily dominated by the seasonal excursion of the ITCZ between 0°N and 10°N, while subtropical region is rather dominated by evaporation with a less marked seasonality (Figures 2a and 2c). In the open ocean, the atmospheric term is dominated by the evaporation-precipitation budget (compare colors and contours). Near the coasts, in particular, where strong salinity variations were noted above, the river runoff appears to play a major role.

Interestingly, the oceanic contribution to MLS variations exhibits a similar spatiotemporal distribution but with an opposite sign as compared to the atmospheric contribution (Figures 2b and 2d): oceanic terms tend to increase mixed layer salinity in the tropics below the ITCZ while they contribute to freshen it in the extratropics. The oceanic contribution is of similar order of magnitude as the atmospheric one, so that the

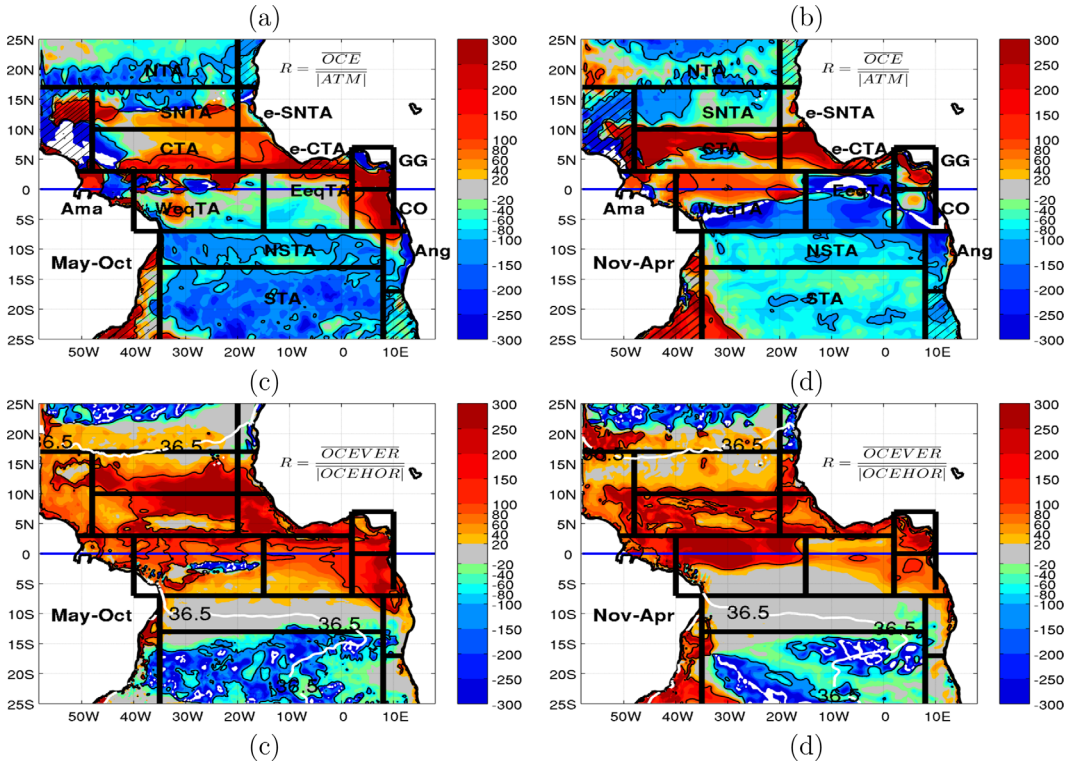

Figure 3. Ratio (in term of percentage) of (a) May–October and (b) November–April averages of the oceanic and the absolute value of atmospheric contributions to MLS variations in the model. (c, d) Same as Figures 3a and 3b between vertical oceanic and absolute value of horizontal oceanic processes. Black continue contours are 100 and −100 values of the ratios. White contours in Figures 3c and 3d are MLS in psu. Hatched areas were not investigated in this study.

total MLS tendency (Figures 1d and 1f) is typically weaker than the individual atmospheric and oceanic terms (Figure 2), especially in the extraequatorial regions. This suggests that the sea surface salinity variability results from the residual of mainly compensating oceanic and atmospheric contributions.

In order to better quantify the relative contribution of oceanic and atmospheric terms, the ratio (expressed in percentage) of the mean oceanic contribution over the absolute value of the mean atmospheric contribution is shown for the May–October period and November–April period (Figures 3a and 3b), respectively. Both the sign and the amplitude of this ratio exhibit strong spatial and temporal variability. Nevertheless, this map highlights the generally strong relative contribution of oceanic processes for the MLS seasonal variability in almost all the basin during both periods, as already underlined in the previous studies [*Da-Allada et al*., 2013; *Yu*, 2011; *Foltz and McPhaden*, 2008; *Mignot and Frankignoul*, 2004]. For example, in boreal summer, below the ITCZ in the northern tropics, ocean processes increase the upper water salinity, with a relative contribution of 60% as compared to atmospheric processes. In the cold eastern equatorial region, during November–April, oceanic terms freshen the surface and their effect on MLS is more than twice as strong as the one of the atmospheric fluxes.

The oceanic contribution can be further partitioned into vertical and horizontal processes. Ratio of both contributions is shown in Figures 3c and 3d. Between 5°S and 15°N, one can note a very strong salting contribution of vertical processes highlighted by the 100% ratio contours and following the seasonality of the ITCZ location. Horizontal processes are rather dominant poleward of these regions and up to the subtropical salinity maxima delineated by the 36.5 psu isohaline. Further poleward of the salinity maxima vertical processes is dominant again but induces a freshening of the mixed layer.

In order to examine these processes in more details, we define 13 regions (black boxes in Figures 3a and 3b) according to the relative homogeneity of the balances of processes driving the MLS as deduced from the ratios in Figure 3. In the following, we describe successively the seasonal evolution of the MLS averaged over these different regions using the decomposition of the salinity budget presented above. For this, and

in order to highlight similarity of processes at play, we will discuss regions where the oceanic dynamics mainly compensate for the evaporative freshwater flux first, and precipitation second. Third, we shall consider regions where oceanic processes compensate each other.

3.2. Evaporative Regions

We first consider the most remote regions relative to the equator of our domain, where the atmospheric flux is dominated by evaporation [*Yu*, 2011]. Two of these regions are located equatorward of the subtropical SSS maxima: the northern tropical Atlantic region (NTA; 17–25°N/58–20°W) and the symmetrical one in the southern hemisphere, which we named the northern south tropical Atlantic region (NSTA; 7–13°S/35°W–8°E). The third one located partly poleward of the south Atlantic SSS maximum is the south tropical Atlantic (STA; 13–25°S/35°W–8°E). In these three regions, the modeled MLS tendency is roughly consistent with the observations with a comparable seasonal cycle lying within the error bar of the data set (Figures 4a, 4c, and 4e black line curves and gray shading). It does not exceed 0.1 psu/month, and it is generally weaker than the individual oceanic or atmospheric contributions. The atmospheric damping term, given by the difference between the total atmospheric contribution and the physical evaporation-precipitation-runoff budget (Figures 4a, 4c, and 4e; solid and star red curves), also shows a negligible contribution in these three regions in comparison to the atmospheric and oceanic contributions. This gives credit to the interpretation of physical processes in this region.

NTA and NSTA have a relatively comparable MLS seasonality (Figures 4a and 4c), except that they are out of phase as they lie in the opposite hemispheres. Note that they are not exactly located at symmetrical latitudes because of the mean northward position of the ITCZ. The atmospheric and oceanic forcing terms indicate that the weak magnitude of the MLS tendency results from compensation between these two terms. The atmospheric physical contribution is positive all year long, illustrating the dominant effect of evaporation, and the oceanic one is negative. Regarding NTA, the strong oceanic effect is consistent with previous studies based on observations [e.g., *Foltz and McPhaden*, 2008] and models [*Qu et al*., 2011]. During the boreal spring and summer (April–September) both the atmospheric and the oceanic terms are maximum, and the resulting MLS tendency is slightly negative, due to an enhanced freshening effect of the oceanic contribution. During winter, the dominant evaporation results in a positive MLS tendency. Horizontal advection (Figure 4b, green) is mainly responsible for the boreal summer maximum freshening. Indeed, in summer, the northeastern wind stress reaches its seasonal maximum in subtropical North Atlantic [*Liu*, 2012; *Qu et al*., 2011] resulting in a maximum Ekman transport of tropical freshwater from the ITCZ (Figure 4b, blue curve) together with a maximum evaporation. During the boreal winter, the wind stress decreases leading to a reduced Ekman transport, which however remains the dominant component of horizontal advection. The phasing of the oceanic and atmospheric contributions is thus explained by the dual effect of the wind which enhances both the evaporation, hence the surface salinity concentration, and the northward Ekman transport of freshwater. The situation is exactly similar in NSTA during austral late summer, when easterlies are maximum in the southern tropics. In both cases, the geostrophic component of advection has a much weaker seasonal cycle, and contributes to increase mixed layer salinity all year long. Indeed, salty water from the maximum salinity areas is advected in NTA and NSTA, respectively, by the negative meridional component of geostrophic currents.

Although of a secondary order, the vertical processes contribute to increase MLS from April to October (during boreal spring-summer), mitigating the Ekman transport of freshwater in the NTA. During this period, we observe an increase of the kz coefficient ($kz \sim 10^{-3.5}\mathrm{m}^2\,\mathrm{s}^{-1}$), an enhanced vertical salinity gradient at the MLD base (Figure 5b), and a reduced MLD. All these three elements contribute to increase the vertical diffusion of salt at the base of the mixed layer. The MLD shallowing is simply a result of the seasonal upper layer stratification due to summer heating, and the vertical salinity gradient results from the Ekman freshwater advection in surface. As explained above, several factors may induce a strong turbulent coefficient, including the direct input of momentum from the winds and/or the Kelvin-Helmholtz instability, characterized by weak Richardson number. Here in spite of a strong shear, in particular from April to October associated to the meridional components of the current (Figure 5c), the Richardson number at the base of the mixed layer remains greater than 10 all year long ($\log(Ri) > 1.5$, Figure 5d, contours). This is possible given the strong stratification at the base of the mixed layer (Figure 5b). The turbulent diffusion coefficient intensification in boreal summer is thus not due to the development of Kelvin-Helmholtz instabilities. We suggest that it is rather a direct consequence of the wind stress intensification (Figure 5a). Interestingly, in NTA, the

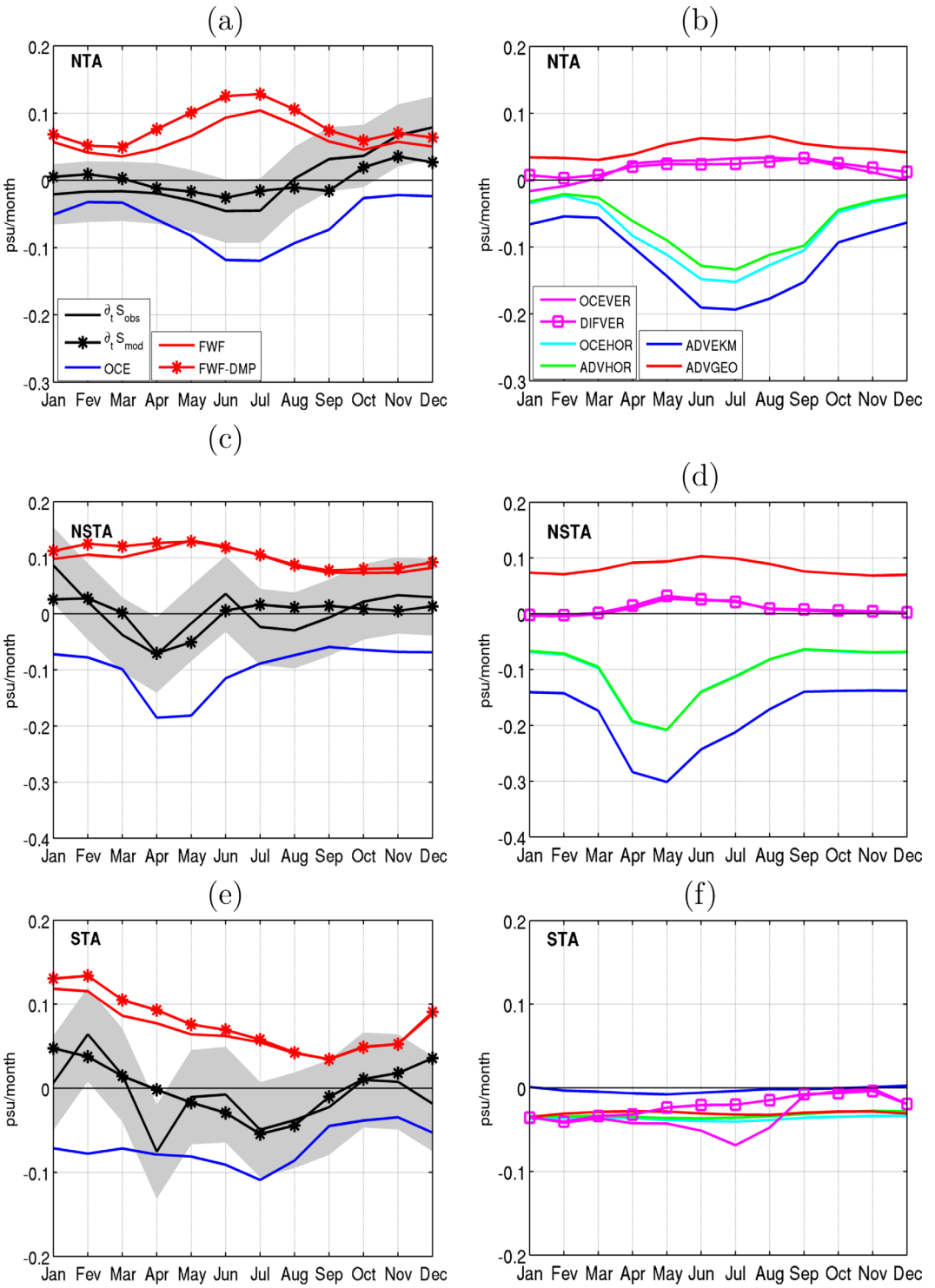

Figure 4. Seasonal evolution of the (a, c, and e) mixed layer salinity budget and (b, d, and f) its components due to ocean dynamics in psu/month averaged over: (Figures 4a and 4b) the NTA region (17:25°N/58:20°W), (Figures 4c and 4d) the NSTA region (13:7°S/35°W:8°E), and (Figures 4e and 4f) the STA region (25:13°S/35 degree W:8°E). In Figure 4d, the cyan curve is overlaid by green line curve. The shaded areas show the estimation of error on data (see text for details). Definitions of the colored lines are given in the legend of the top plot, see text for details.

seasonal cycle of all dominant terms for the MLS budget, namely atmospheric evaporation, Ekman advection of freshwater and vertical diffusion of salt at the base of the mixed layer are all phased by the seasonal cycle of the wind stress. The mechanism is symmetrical in SNTA (not shown).

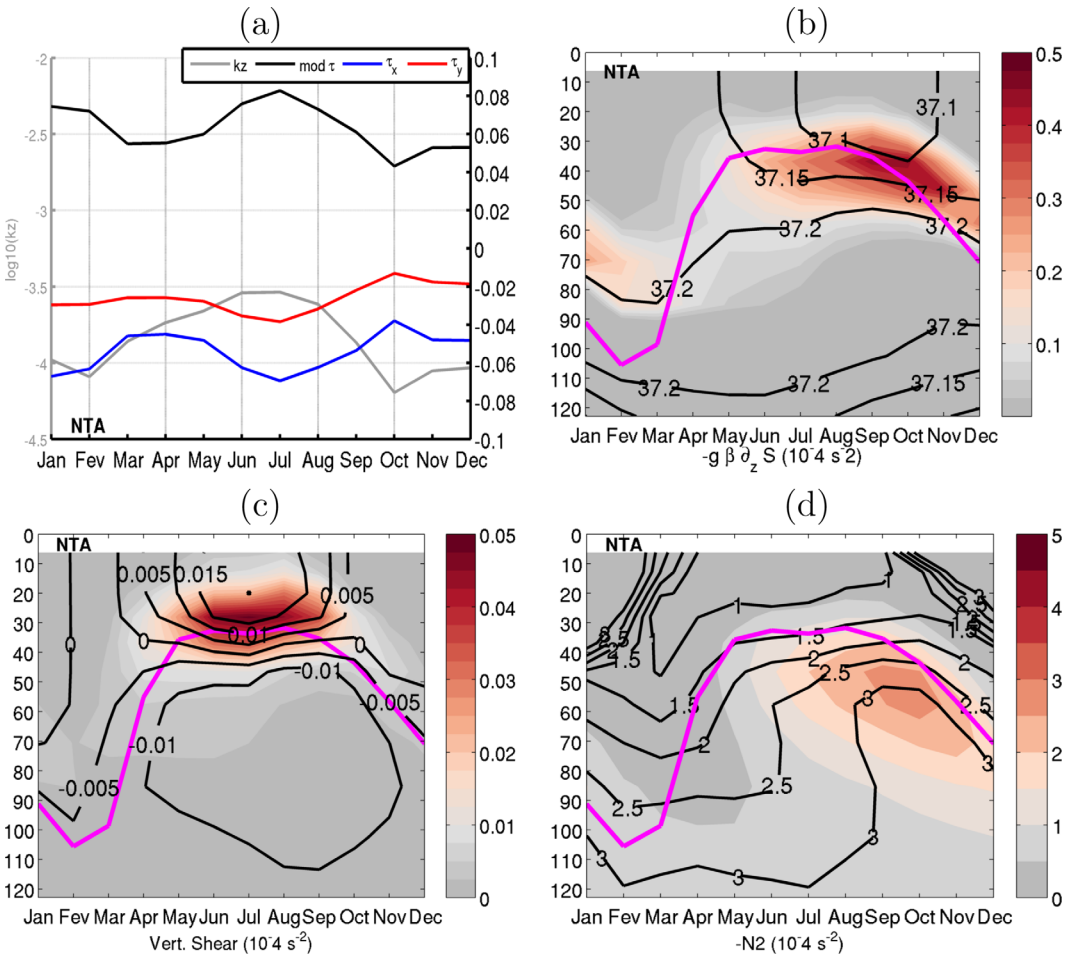

Figure 5. Seasonal evolution for the NTA region. (a) Left axis is the logarithm of the vertical coefficient diffusion at the ML base in $m^2\ s^{-1}$ (gray color; 5 days values higher than 0.1 have not been considered), right axis of is the winds stress in $N\ m^{-2}$ (black is the module, blue is the zonal component, and red is the meridional component). (b) Vertical salinity stratification contribution on Brunt-Väisälä frequency in s^{-2}. Contours show the average salinity. (c) Vertical shear in s^{-2}. Contours show the meridional currents. (d) Vertical Brunt-Väisälä frequency in s^{-2}. Contours show the logarithm of the averaged Richardson number. The magenta curve in Figures 5b, 5c, and 5d is the mixed layer depth in m.

The southern tropical Atlantic (STA; 13:25°S/35°W:8°E) is located southward of the subtropical salinity maximum. As for the NTA and NSTA, the MLS tendency is relatively weak and results from opposite contributions of the atmosphere and the ocean. However, in contrast with NTA and NSTA, the effect of Ekman transport is negligible, as its currents are parallel to isohaline (not shown). The geostrophic term here is negative and practically constant all year long (Figure 4f, red). It is due to a transport of low saline water from the eastern boundary upwelling by the southern branch of the SEC (Figures 1a and 1b). The seasonality of the total oceanic contribution is primarily due to the vertical terms (Figure 4f), which cannot be explained by vertical diffusion alone (Figure 4f). The latter is maximum in austral summer, when the wind stress enhances vertical mixing, as described above for NTA. However, in this region, the vertical salinity gradient at the base of the mixed layer is positive (Figure 6a). As a result, vertical diffusion contributes to freshen the mixed layer, unlike for the regions located on the equatorward flank of the surface salinity maximum (SSM) and described above. Contrary to NTA and SNTA, the entrainment term also appears to play a strong role for the MLS budget during the austral winter season, as the mixed layer deepens. (Figure 6, magenta curve). During the deepening phase of the ML, the density vertical gradient at the base of the mixed layer is weak in this region in spite of a maximum salinity (and temperature, not shown) gradient because temperature and salinity are compensated (Figures 6a–6c): as mentioned above, the regions poleward of the SSM are characterized by a destabilizing vertical salinity gradient [*Liu et al.*, 2009; *Yeager and Large*, 2007]. Under the effect of winter heat loss, convective mixing operates, strongly deepening the mixed layer, thereby entraining

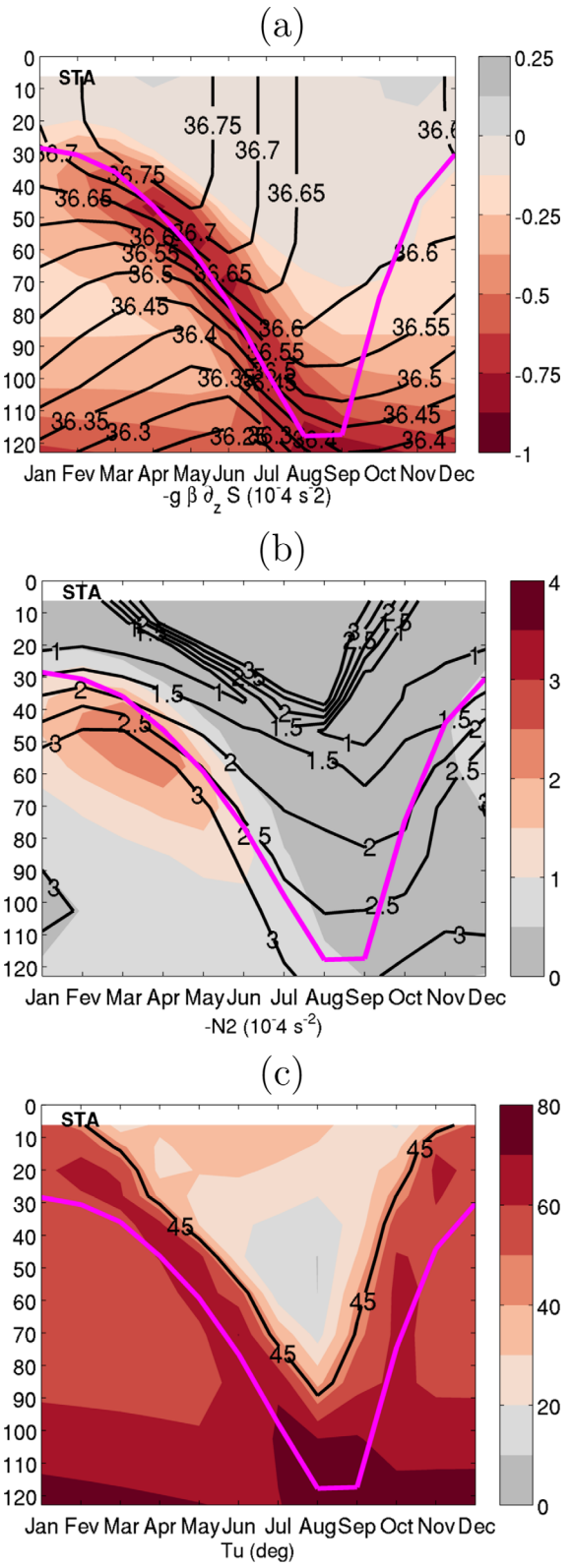

Figure 6. Seasonal evolution of vertical profiles for the STA region. (a) Vertical salinity stratification contribution on Brunt-Väisälä frequency in s^{-2}. Contours show average salinity. (b) Vertical Brunt-Väisälä frequency in s^{-2}. Contours show the logarithm of the averaged Richardson number. (c) Turner angle in °. The turner angle 45° is highlighted in black contour.

relatively fresh waters into the mixed layer. This process is responsible for the formation of a Strongly Density Compensated (SDC) layer characterized by high turner angle values greater than 45° at the base of the mixed layer (Figure 6c). These effects have been described in subtropical regions of the Pacific and Atlantic [*Kolodziejczyk et al.*, 2014a; *Kolodziejczyk and Gaillard*, 2013; *Yeager and Large*, 2007].

To conclude, these three subtropical regions are characterized by a freshening effect of the ocean compensating for the atmospheric evaporation. In NTA and NSTA, located equatorward of the SSM, this effect is primarily due to the poleward Ekman transport of fresher waters with a weaker mitigating effect of the vertical turbulent diffusion. All these terms are maximum in summer because of the wind intensification. In STA, the vertical diffusion also peaks in phase with the maximum evaporation but it is this time directly opposing the latter as the vertical salinity gradient is reversed. The summer MLS balance thus here essentially plays between evaporation and vertical diffusion together with geostrophic fresh transport. Furthermore, during austral winter in STA, the oceanic contribution to freshening of the mixed layer is reinforced and dominated by vertical convective entrainment due to strong winter heat loss associated with destabilizing (negative) vertical salinity gradient located poleward of SSM.

3.3. Region of Precipitation and Rivers Runoff

3.3.1. Region of Precipitation

We focus here on regions of the tropical Atlantic associated with intense precipitations. The ITCZ is located over the geographical equator in boreal early spring, and in particular over the western equatorial Atlantic (WeqTA, 7°S:3°N/

40°W:15°W). Then, it migrates northward (Figure 2a), thereby reaching the central tropical Atlantic (CTA, 3°N:10°N/48°W:20°W and its coastal extension e-CTA, 3°N:10°N/20°W:14°W) between May and October, and finally the southern-north tropical Atlantic around 15°N, here represented as the SNTA region (10:17°N/48°W:20°W) in August. Around September, the ITCZ starts its southward migration. It passes over the central tropical Atlantic a second time in fall and reaches again the equator in boreal winter. Figures 7a and 7g clearly show a freshening of the MLS due to a negative contribution of the E-P flux associated with ITCZ-induced rainfalls over the western equatorial tropical Atlantic in early spring and the southern part of the north tropical Atlantic in August, respectively. During the rest of the year, these regions are rather weakly evaporative. In e-CTA (Figure 7e), the precipitation dominates the evaporation throughout the year with a semiannual cycle, consistently with the double passage of the ITCZ, while further west (CTA, Figure 7c) the atmospheric freshening shows no interruption from May to December. Note that, in this latter region, the damping term diagnosed from the difference between the physical atmospheric forcing and the total forcing imposed in the model (red curves in Figure 7c) is relatively strong, in particular from May to October, thereby limiting the quantitative interpretation of physical processes simulated by the model and possibly the semiannual cycle due the ITCZ. This may be due to uncertainties in the forcing precipitation data or in the salinity data (gray shading in Figure 7c), which are used to diagnose the damping term in the simulation. Large uncertainty on data in this region is illustrated by the gray shading. In all these regions again, strong oceanic contribution opposes the atmospheric one. This strong ocean contribution was also found by *Foltz et al*. [2004, 2015], mainly in the central part. Figure 7 (right) shows that both horizontal and vertical oceanic terms play a comparable role. At the west equator, the SEC advects fresher waters from east following a semiannual cycle peaking in June and December [*Richardson and McKee*, 1984], but this effect is counteracted by the meridional advection effect. It results in a mitigated semiannual freshening by the horizontal advection peaking in August and December. Further north, horizontal processes are weak as long as the ITCZ is located south of the respective areas, and dominated by a weak freshening due to anomalous northward Ekman advection of equatorial fresh water. An abrupt change in the sign of the Ekman contribution is detected in June in CTA, as the ITCZ moves northward of this area: Ekman currents become southward and then rather export freshwater out of the region. An abrupt modification of the geostrophic advection is concomitant, as the wind stress curl associated with the meridional shift of the ITCZ and Azores High triggers the North Equatorial Counter Current (NECC) and the NEC [*Bourlès et al*., 1999; *Richardson and McKee*, 1984]. The resulting geostrophic advection of the fresh Amazon waters from the west toward the central tropical Atlantic [*Yang and Joyce*, 2006; *Dessier and Donguy*, 1994; *Muller-Karger et al*., 1988] mainly contributes to counteract the Ekman current effect. Similar seasonality is found further east (e-CTA) but for the relative strength of geostrophic and Ekman advection, so that the resulting effect of horizontal advection is rather a net salting (Figure 7f). Finally, the SNTA is not affected by such change of direction of Ekman currents because the ITCZ does not shift north of this region. Yet in boreal fall and winter, as the ITCZ is located right at the southern edge of this area, salinity gradients are intense, which explains the strong Ekman contribution to the MLS budget, consistently with *Mignot et al*. [2007]. Thus, in all these regions, horizontal oceanic contribution is tightly linked to the wind convergence associated to the ITCZ location and thus also to atmospheric precipitations.

In these strong precipitation regions, vertical processes, dominated by vertical salinity diffusion, have a strong salting effect on the MLS (Figure 7, right). The vertical diffusion term has a marked seasonal cycle, again clearly phase locked with the other processes. In WeqTA, it reaches its maximum in April (Figure 7b, magenta squared curve). This maximum is concomitant with a strong salinity stratification, due to the surface intense precipitations, and a minimum MLD. On the other hand, the seasonality of the diffusion coefficient kz (Figure 8a) is clearly antiphased with the total vertical diffusion term: it is minimum in boreal spring, when the latter is maximum and maximum in boreal fall. This confirms that the vertical salinity gradient and the spring mixed layer shallowing are responsible for the vertical diffusion phasing with the other components of the MLS budget. Yet the fact that the total vertical diffusion is antiphased with the vertical diffusion coefficient may seem surprising. The seasonal cycle of the latter is set by the wind-induced turbulence, as seen in Figure 8a. Nevertheless, note that, in spite of this seasonality, the vertical diffusion coefficient is all year long relatively strong: its yearly average amounts $10^{-3} m^2 s^{-1}$, which is the strongest value as compared to what is found in all the other regions (compare with Figure 5a, for example). This is consistent with a relatively low Richardson number all year long (Figure 8d) indicating that conditions are

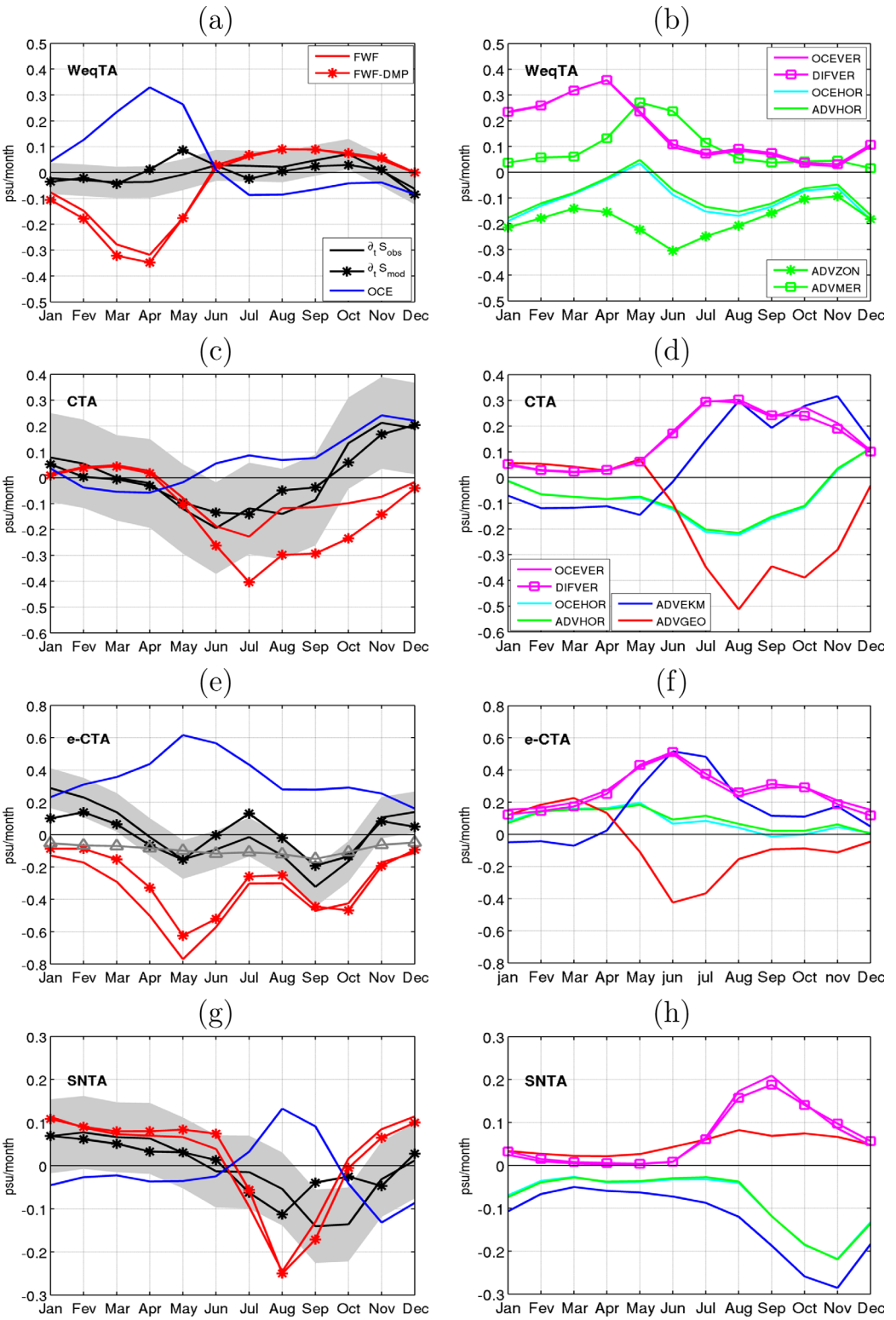

Figure 7. As Figure 4 except for (b) where horizontal advection is separated into zonal and meridional components: WeqTA (7°S:3°N/40:15°W), CTA (3:10°N/48:20°W), e-CTA (3:10°N/20:14°W), and SNTA (10:17°N/48:20°W).

favorable for shear turbulence. The vertical shear of horizontal currents (Figure 8c), resulting from the westward SEC flowing above the eastward EUC, is indeed strong. It is maximum in late spring, when the SEC intensifies, but it is then largely balanced by the vertical stratification essentially due to salinity.

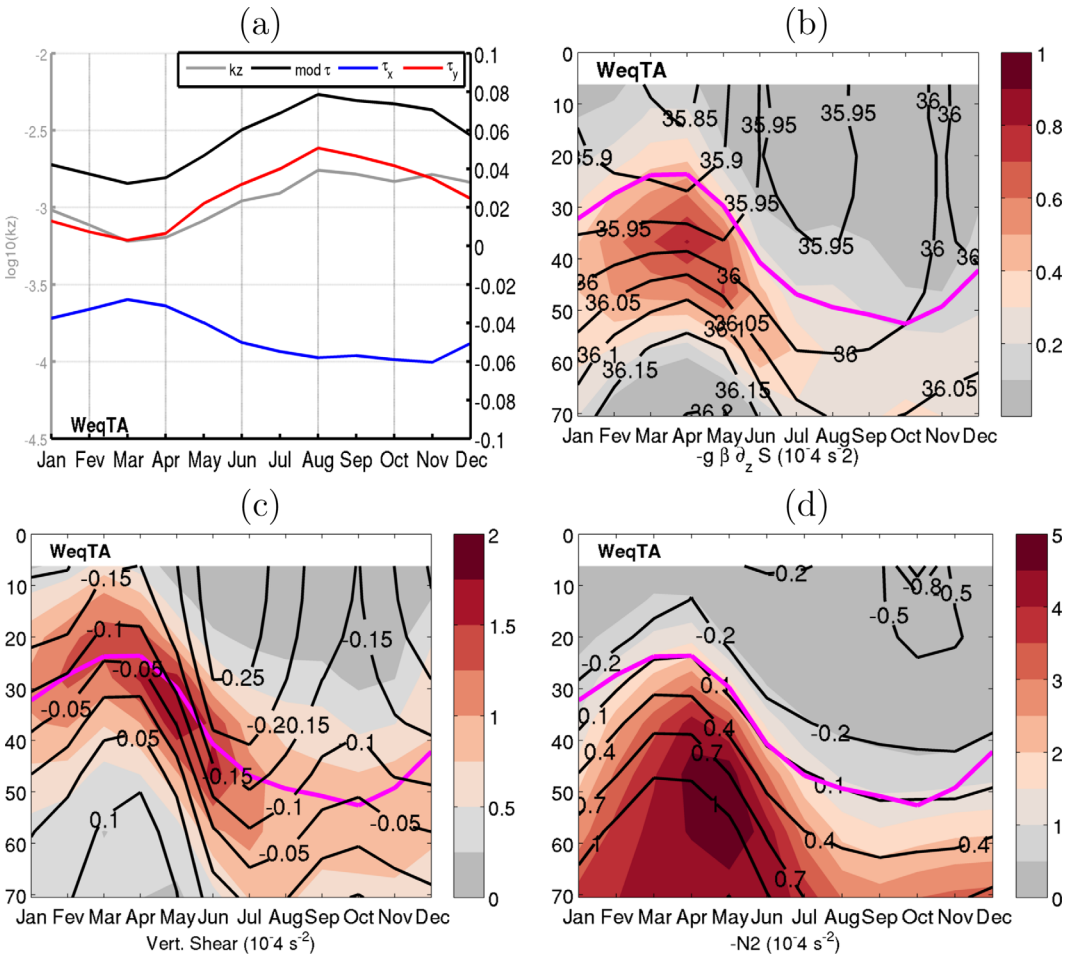

Figure 8. As Figure 5 at WeqTA (7°S:3°N/40:15°W).

To summarize, the west equatorial Atlantic is characterized by large values of the vertical diffusion coefficient as a result of a strong horizontal shear. In spring, when surface precipitations induce a strong vertical salinity gradient at the base of the mixed layer, this allows vertical diffusion to evacuate very efficiently this fresh water toward the ocean interior via shear-induced turbulence. Note that the impact of shear instabilities was also reported in *Jouanno et al.* [2011] using another numerical simulation. The latter focused on the equatorial band only, and found much weaker values of the Richardson number. Here the Richardson number also falls below the instability criterion (1/4) between 40 and 10 W in May–June along the Equator. The use of the regional average masks local extreme values. In the three other regions influenced by the ITCZ, the vertical dynamical shear is not as strong as in the WeqTA. Nevertheless, processes are similar: the vertical diffusion is strongly enhanced when the salinity gradient is maximum under the ITCZ (not shown).

3.3.2. River Runoff Regions

We briefly review here three coastal regions which follow similar processes as the ones described above except that the strong freshwater flux is mainly supplied by rivers runoff (Figures 9a and 9c, gray triangle curve). These are the region of the Amazon outflow (Ama, 7°S:3°N/51:40°W), the eastern southern-north tropical Atlantic (e-SNTA, 10:17°N/20:12°W), and the Gulf of Guinea (GG; 0:7°N/2:10°N). Note that since *Da-Allada et al.* [2014, 2013] already investigated the GG region, we focus here on the two former ones. In Ama, the freshwater flux is totally due to the Amazon outflow which reaches its maximum in June (6 psu/month). It is about 10 times stronger than typical trends detected in other regions of the tropical Atlantic. On the other side of the ocean, off the Senegal and Guinean coasts, the freshwater flux reaches its maximum in boreal fall, both because the ITCZ has reached its northernmost position and because of large outflow from

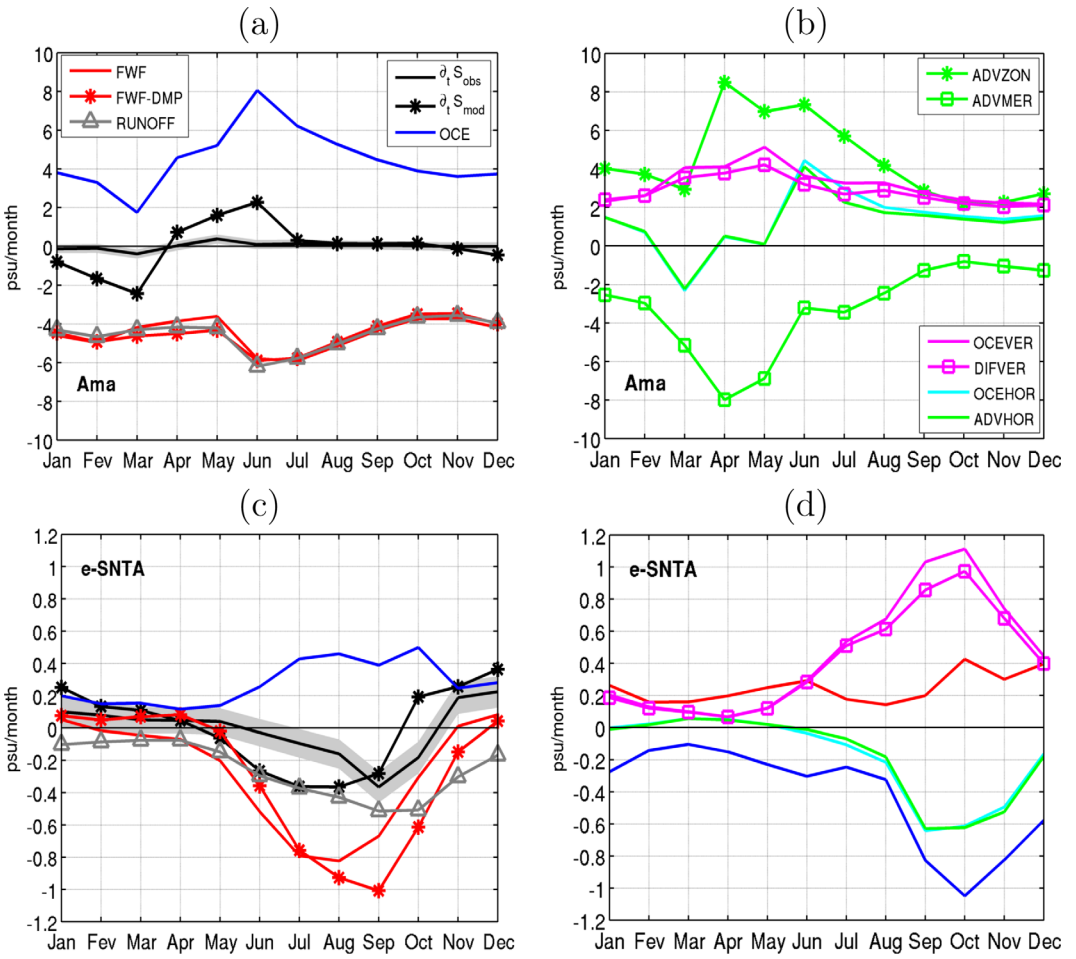

Figure 9. As Figure 4 except for (b) where horizontal advection is separated into zonal and meridional components: Ama (3°N:7°S/51:40°G) and e-SNTA (10:17°N/20:5°W). Units are in psu/month.

the Senegal and Gambia rivers. Interestingly, the resulting atmospheric freshening is maximum in September that is 1 month later than in the adjacent SNTA region. In these two regions, the total salinity variations have difficulties following the observations. The modeled variations are indeed partly out of the range of observations. This could be due to biases in precipitation and evaporation reconstructions [*Trenberth et al*., 2001; *Trenberth and Guillemot*, 1998], biases in the observed SSS data set, since these areas are poorly sampled with data or an underestimation of the mixed layer depth because of the use of a small density criterion (0.01 kg m^{-3}) which could lead to an overestimation of the tendency. In any case, we note that it does not induce a change of sign and seasonality of the physical atmospheric forcing term, so we believe that these regions can be qualitatively interpreted. In both regions, the ocean acts to damp atmospheric and river freshwater inputs, and the resulting MLS tendency is roughly an order of magnitude weaker than the atmospheric and oceanic individual contributions. As for the regions located in the open ocean (section 3.3.1), the sign of the oceanic contribution is set by the salting effect of the vertical salinity diffusion at the mixed layer base (Figures 9b and 9d), which works to evacuate the surface freshwater toward the ocean interior. The seasonality of the vertical diffusion is strongly locked to the upper salinity stratification (not shown). Horizontal advection contributes to freshen the mixed layer in e-SNTA practically all year long, with a strong Ekman contribution in fall when the ITCZ reaches this area, as for the adjacent SNTA region. Near the Amazon river's mouth, zonal and meridional components generally compensate, with a dominant effect of the zonal component of the NBC in summer.

To conclude, the northern tropical Atlantic region, from the equator to the southern edge of the northern subtropical SSS maximum, is characterized by a marked seasonal effect of precipitations, following the seasonality of the ITCZ, and associated rivers runoff in well-known coastal regions. Both effects generate strong

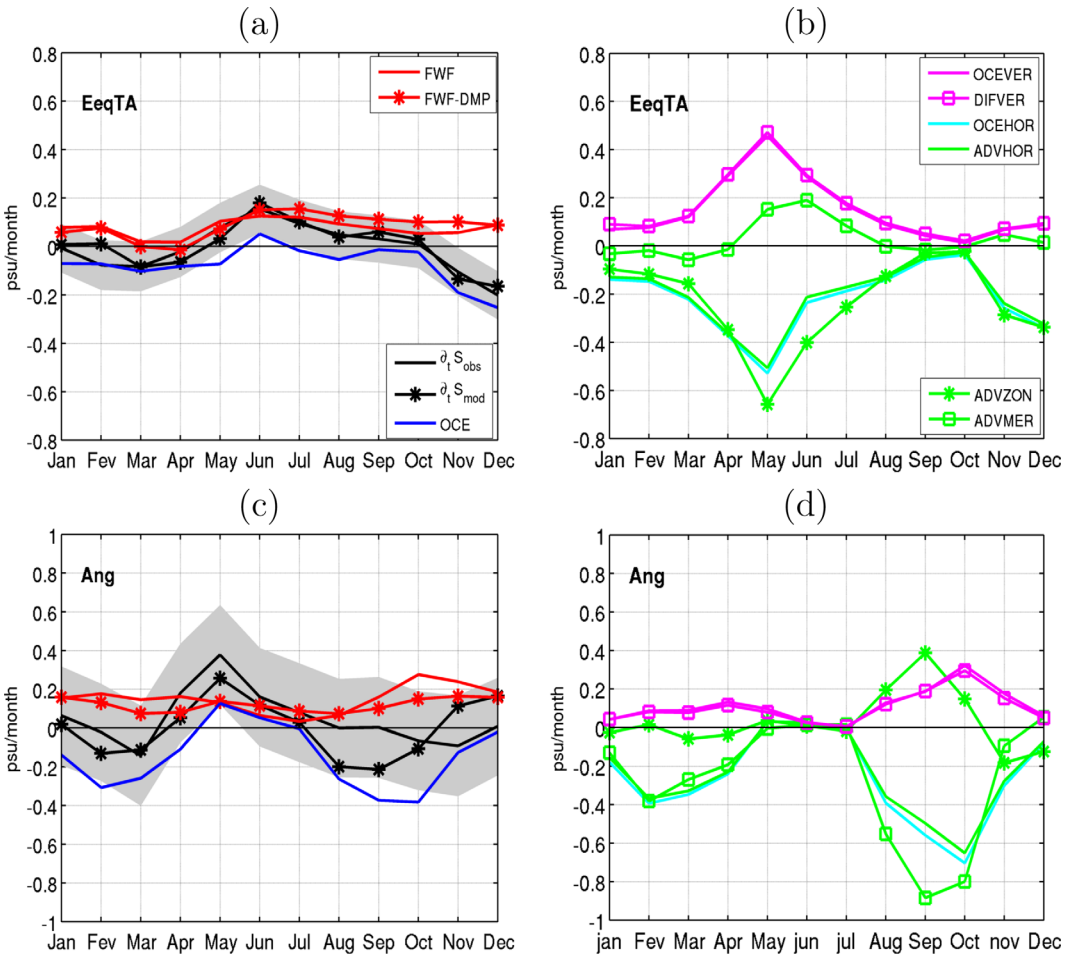

Figure 10. As Figure 4 at EeqTA (7°S:3°N/15°W:2°E) and Ang (7:17°S/8:14°E).

vertical salinity gradient at the base of the mixed layer. The ocean responds by reducing this strong seasonal vertical salinity gradient through enhanced vertical diffusion. The horizontal advection acts to export or import (redistribute) the surface freshwater, while the vertical diffusion always acts to evacuate the freshwater toward the ocean interior. Evaporation is mainly due the salinity stratification concomitant with MLD shallowing. Especially at the equator where shear is developed, the vertical mixing contributes also strong on the subsurface water freshening.

3.4. Regions Dominated by Oceanic Processes

We finally discuss the eastern tropical Atlantic where the MLS variability is driven by very different processes from the ones discussed above. In the eastern equatorial region (EeqTA, 15°W:2°E/7°S:3°N, Figures 10a and 10b) and the coastal region along Angola (Ang, 17:7°S/8:14°E, Figures 10c and 10d), the atmospheric and oceanic contributions to the MLS are both relatively small and of similar amplitude as the total MLS tendency. However, the oceanic contribution results from a compensation between strong vertical and horizontal terms. Both of these follow remarkable semiannual cycles which are practically antiphased. Horizontal advection induces a freshening all year long. In the eastern equatorial Atlantic, it is due to the westward transport of freshwater from the Niger and Congo rivers by the SEC. The semiannual cycle of the latter is driven by the semiannual cycle of the zonal equatorial wind stress as shown in the previous studies [*Ding et al.*, 2009; *Thierry et al.*, 2004; *Richardson and McKee*, 1984]. These winds force the equatorial wave reflection and adjustment which connect the equator to the southern coastal region [*Ding et al.*, 2009; *Philander and Pacanowski*, 1986; *du Penhoat and Treguier*, 1985]. In the latter region, the alongshore Angola Current (AC) transports fresh coastal water from the Congo river mouth [*Gordon and Bosley*, 1991].

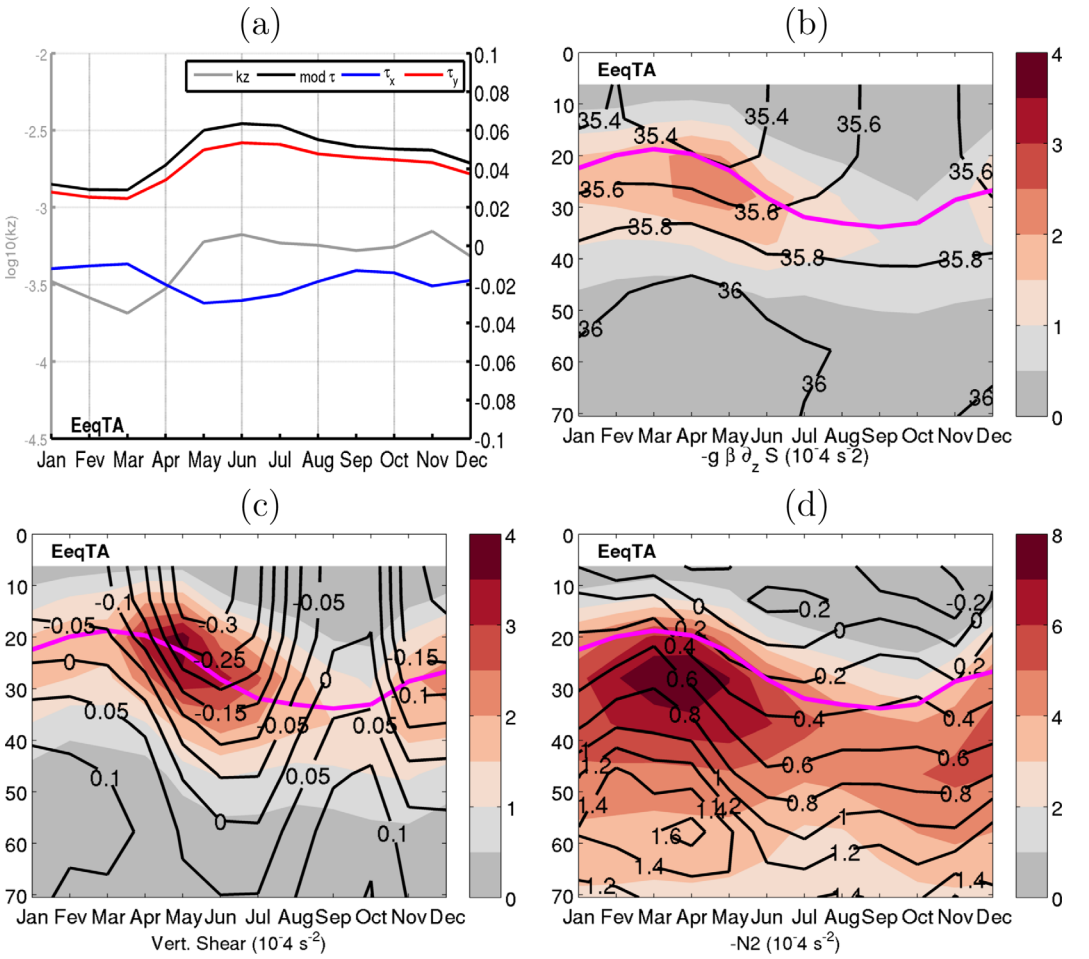

Figure 11. As Figure 5 at EeqTA (7°S:3°N/15°W:2°E).

As in precipitation and runoff regions, the vertical salinity diffusion, dominant vertical process, induces a salting of the mixed layer in Ang and EeqTA region. In the latter, the diffusion increases from January to May, decreases until October and finally reincreases the rest year (Figure 10b). This cycle is in phase with vertical salinity gradient at MLD base and shear (Figures 11b and 11c). The shear is of same order of magnitude as the stratification yielding the small Richardson number (Figure 11d, color and contours). So it suggests that the turbulent salt flux is driven by the vertical shear associated with the strong salinity stratification. The latter increases from late fall to spring as a result of the surface freshening inducing by SEC offshore transport of fresh coastal water and decreases the rest year. The latter, consistently with the semiannual westward strengthening of the SEC, follows a semiannual cycle in the equatorial region with a maximum in spring and fall. During these periods, the shallow strong subsurface eastward EUC also contributes to the enhancement of the shear as also discussed by *Jouanno et al*. [2011] and *Kolodziejczyk et al*. [2014b, 2009]. Note that our so calling small Ri is greater than 0.25 probably because of the use of monthly box averages of vertical shear and stratification and also as explained in WeqTA region. Previous studies, using higher temporal resolution simulations, have indeed shown the role of the vertical shear in setting vertical mixing in these regions [e.g., *Jouanno et al*., 2012, 2011]. This is also consistent with *Foltz et al*. [2013] at 0.23°W. Concerning the vertical coefficient diffusion at the base of the MLD, it increases from March to June (1 month after the maximum diffusion), decreases until September and reincreases until November. The kz variability depends here on wind stress (Figure 11a) which controls the shear via the SEC. In the Ang region, the vertical shear is weaker, and the vertical term seasonality is rather controlled by the effect of vertical salinity gradient mainly (not shown).

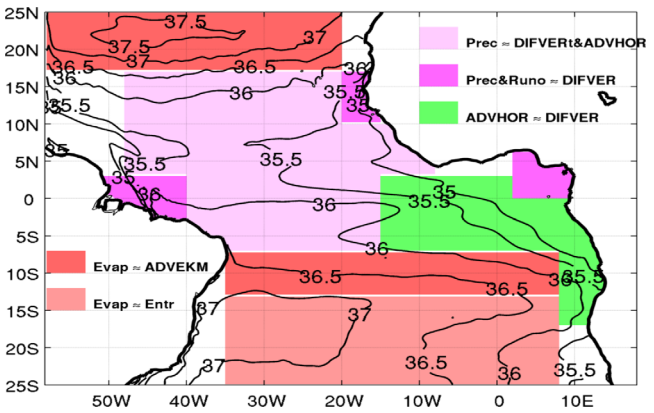

Figure 12. Summary of the main compensating processes influencing the seasonal variability of the mixed layer salinity. Compensation between: evaporation and Ekman advection (red color), evaporation and entrainment (red light), precipitation + runoff and vertical diffusion (magenta), precipitation and vertical diffusion (magenta light), and horizontal advection and vertical diffusion (green). Contours are annual mean MLS in psu.

The coastal region in the vicinity of the Congo river (CO; 2:10°E/7°S:0) follows similar processes as the ones at play here, as already analyzed by *Da-Allada et al*. [2014] and *Berger et al*. [2014]. Although *Hummels et al*. [2014] indicates that strongest turbulence is expected to be found in the eastern equatorial region, vertical diffusion in the Congo vicinity is much stronger than in EeqTA in our simulation. This is probably due to a shallower mixed layer and stronger vertical salinity gradient in the Congo than the eastern equatorial areas, explained by the presence of Congo plume [*Vic et al*., 2013] thus the vertical diffusion effect is integrated over a larger depth in EeqTA and its net effect is weaker than in CO.

4. Summary and Discussions

We have diagnosed the seasonal cycle of the mixed layer salinity in the tropical Atlantic from a regional oceanic general circulation model using climatological forcing. This study shows that the seasonal variations of salinity in the mixed layer are noticeably weaker than individual contributions from atmospheric and oceanic forcing. In the subtropical and tropical Atlantic, the oceanic dynamics generally adjusts to the freshwater forcing from the atmosphere, runoff and/or precipitation so that salinity variations are strongly damped. Three main regions corresponding to the dominant freshwater forcing could be identified and described, taking into account these compensation processes (Figure 12).

In the dominantly evaporative regions of the tropics and subtropics (Figure 12, red and light red areas), the general increase of salinity in the mixed layer due to persistent evaporation is largely compensated by the oceanic dynamics, which strongly contributes to modulate the MLS seasonal variability and thus subtly maintains the horizontal distribution of the SSS [*Hasson et al*., 2013a, 2013b]. The seasonal cycle of evaporation is driven by the wind stress intensification in the local summer season. On the equatorward flanks of the subtropical SSS maxima, the wind stress also induces a poleward Ekman transport of freshwater which mitigates the effect of the atmosphere all year long. Atmospheric evaporation and Ekman transport are thus coupled through the influence of the winds [*Han et al*., 2001]. Vertical diffusion and geostrophic transport contribute on the other hand to the salting of the mixed layer but they are playing a weaker role. Poleward of the southern SSS maxima (only investigated in the southern hemisphere in this study), the Ekman transport is very weak on average, only the geostrophic transport and the vertical diffusion, this time with a negative effect, counteract the effect of intense evaporation. In winter, convection adds on the geostrophic advection, inducing a significant input of low salty water from the subsurface into the mixed layer [*Kolodziejczyk and Gaillard*, 2013; *Yeager and Large*, 2007] which interannual variability contributes to ventilate salinity anomalies in the ocean interior [*Kolodziejczyk and Gaillard*, 2013; *Qu et al*., 2013; *Laurian et al*., 2009]. These results reveal a complex interplay between atmospheric and oceanic salinity flux at seasonal scale, which results in the lack of a direct relationship between freshwater flux and MLS, consistently with *Vinogradova and Ponte* [2013]. A direct relationship between freshwater forcing and MLS is rather found at

longer time scales, i.e., interannual to decadal scale [*Vinogradova and Ponte*, 2013; *Durack et al*., 2012; *Terray et al*., 2012].

Under the seasonal march of the ITCZ and in coastal areas affected by river runoffs (Figure 12, magenta and light magenta areas), the effect of the strong precipitations is strongly counteracted by salting oceanic contributions, mainly through vertical mixing, which also results in a small net MLS tendency in comparison to individual forcing. In the central basin, from 5°N to the southern edge of the northern SSS maximum, the MLS variations are nevertheless following the precipitation variations, consistently with *Yu* [2011]. The freshening is, however, strongly attenuated by the vertical diffusion of salt at the base of the mixed layer, so that the accuracy of considering salinity as a good proxy for precipitations in this area is again questionable, as also discussed in *Vinogradova and Ponte* [2013]. The vertical diffusion is essentially the consequence of the strong vertical salinity gradient at MLD base which is maximum during rainy season, while turbulence itself is not strongly developed except along the equator. Note that off equator, anomalous Ekman transport strongly contributes to freshen (salt), the region when the ITCZ is located further equatorward (poleward), and the anomalous geostrophic contribution is always opposed to the Ekman transport effect. In these regions, the strong surface freshening also allows the formation of thick seasonal barrier layers [e.g., *Mignot et al*., 2012], which play an important role for the thermal heat budget. On the other hand, the diffusion at the base of the mixed layer contributes to inject freshwater in the interior of the ocean thereby destroying the barrier layer [*Akhil et al*., 2014]. The contribution of the vertical term is usually underestimated in observational studies [e.g., *Yu*, 2011], thus poorly discussed. In this study, the model has allowed us to assess consistent estimates and infer which processes may be responsible for the strong vertical salt flux at the base of the ML.

Finally, the eastern tropical Atlantic (Figure 12, green area) is characterized by a strong oceanic dynamics, with a weaker effect of atmospheric fluxes. Freshwater from the discharge of the Congo and Niger rivers are advected westward by the SEC following a semiannual cycle. This region is furthermore characterized by the persistent eastward EUC, hence a quasipermanent vertical shear of the horizontal currents. Associated with the strong salinity stratification, this favors a strong semiannual vertical turbulent diffusion of salinity which largely compensates the surface freshwater advection. This results once more in weak MLS seasonal variations, although individual contributions may be large. These results are in agreement with previous studies based on observations and models [*Berger et al*., 2014; *Da-Allada et al*., 2014, 2013].

The present study did not address the intraseasonal ocean dynamics which could strongly modulate the vertical shear of the horizontal currents in the equatorial regions. Previous studies have shown that intraseasonal wind variability [*Marin et al*., 2009], equatorial wave dynamics [*Jouanno and Sheinbaum*, 2013; *Hu and Huang*, 2007; *Handoh and Bigg*, 2000] or TIWs [*Athie and Marin*, 2008; *Peter et al*., 2006] could affect the vertical turbulent mixing of heat and modulate the heat flux between the ML and interior ocean [*Jouanno and Sheinbaum*, 2013; *Jouanno et al*., 2012; *Wade et al*., 2011]. Further work is needed to address the shorter term variability of the MLS.

Although largely consistent with previous studies, our study has some limitations, in particular linked to the use of the model. First, the nominal oceanic resolution is only 0.25°. This is in general not to accurately represent the role of mesoscale eddies. The latter have recently been shown to play a fundamental role in transient ocean heat uptake [*Griffies et al*., 2015], it is most certainly also the case for the haline budget. The salinity restoring is also of course an important issue while investigating the upper ocean salinity budget. As discussed in *Griffies et al*. [2009], this term is needed in ocean only configurations because of the lack of many feedbacks due to the absence of an active atmospheric component and because of the absence of local feedbacks between SSS and freshwater fluxes that can lead to unbounded local salinity trends in response to inaccuracies in precipitation. Several studies have shown that the salinity restoring can strongly affect the oceanic mean state [e.g., *Large et al*., 1997], but the impact on the strength of the restoring on the oceanic mean state is itself not clear and perhaps partly model dependent. For example, while a stronger restoring produces larger transports associated to the Atlantic meridional overturning circulation in *Behrens et al*. [2013], opposite relationship is found in the NCAR model, as discussed in *Danabasoglu et al*. [2014]. Furthermore, here, we have shown that the damping term is generally relatively small as compared to the physical atmospheric fluxes even though in specific regions such as the central tropical Atlantic, it can amount 50% of the physical term. However, it never induces a change a sign of the total freshwater flux so that we consider our conclusions to be generally robust. Another limitation of our study is the use of

climatological forcing. Such configuration has been used in several previous studies [e.g., *Marsland et al*., 2003]. The impact of using interannual forcing on the climatological salinity upper ocean budget has not been addressed here.

Our study has highlighted that the vertical salinity diffusion is an important component of the upper ocean salinity budget in most areas of the tropical Atlantic. This may explain the difficulties of previous observational studies like *Da-Allada et al*. [2013] and *Foltz and McPhaden* [2008] to close the ML salinity budget in some regions. This result may have important consequences for our understanding of the transmission of signals within the ocean interior, vertical dynamic inducing strong flux exchange between the upper and interior ocean. Here we have shown that in spite of weak seasonal variations of the SSS, strong signals, of salinity can be injected at the base of the mixed layer through vertical diffusion. Temperature signals of similar magnitude are also injected through similar processes (not shown). These signals are the major vector of the mid-term to long-term climatic memory of the ocean [*Haarsma et al*., 2011; *Laurian et al*., 2006; *Levitus et al*., 2005; *Vellinga and Wu*, 2004; *Latif et al*., 2000].

Acknowledgments

SSS observations were obtained from the French SSS observation service and are available at http://www.legos.obs-mip.fr/observations/sss. Surface current observations are available at http://www.aoml.noaa.gov/phod/dac/drifter_climatology.html. To access model outputs send a mail at ibrahima1.camara@ucad.edu.sn. The research leading to these results has received funding from Agence Universitaire de la Francophonie (AUF) and the European Union Seventh Framework Programme (FP7/2007–2013) under grant agreement 603521 for the PREFACE project. The authors also acknowledge support from the Laboratoire Mixte International ECLAIRS, funded by IRD. We thank Malick Wade who provided us routines for calculating vertical coefficient diffusion at the mixed layer base. N. K. was funded by French Space Agency (CNES) grant.

References

Akhil, V. P., F. Durand, M. Lengaigne, J. Vialard, M. G. Keerthi, V. V. Gopalakrishna, C. Deltel, F. Papa, and C. de Boyer Montgut (2014), A modeling study of the processes of surface salinity seasonal cycle in the Bay of Bengal, *J. Geophys. Res. Oceans*, *119*, 3926–3947, doi:10.1002/2013JC009632.

Athie, G., and F. Marin (2008), Cross-equatorial structure and temporal modulation of intraseasonal variability at the surface of the tropical Atlantic Ocean, *J. Geophys. Res.*, *113*, C08020, doi:10.1029/2007JC004332.

Balaguru, K., P. Chang, R. Saravanan, and C. J. Jang (2012), The barrier layer of the Atlantic warm pool: Formation mechanism and influence on the mean climate, *Tellus, Ser. A*, *64*, 1–17, doi:10.3402/tellusa.v64i0.18162.

Behrens, E., A. Biastoch, and C. W. Bning (2013), Spurious AMOC trends in global ocean sea-ice models related to subarctic freshwater forcing, *Ocean Modell.*, *69*, 39–49, doi:10.1016/j.ocemod.2013.05.004.

Berger, H., A. Treguier, N. Perenne, and C. Talandier (2014), Dynamical contribution to sea surface salinity variations in the eastern Gulf of Guinea based on numerical modelling, *Clim. Dyn.*, *43*(11), 3105–3122, doi:10.1007/s00382-014-2195-4.

Bingham, F. M., G. R. Foltz, and M. J. McPhaden (2012), Characteristics of the seasonal cycle of surface layer salinity in the global ocean, *Ocean Sci. Discuss.*, *8*(5), 915–929, doi:10.5194/os-8-915-2012.

Bourlès, B., Y. Gouriou, and R. Chuchla (1999), On the circulation in the upper layer of the western equatorial Atlantic, *J. Geophys. Res.*, *104*(C9), 21,151–21,170, doi:10.1029/1999JC900058.

Bretherton, F. P., R. E. Davis, and C. Fandry (1976), A technique for objective analysis and design of oceanographic experiments applied to mode-73, *Deep Sea Res. Oceanogr. Abstr.*, *23*(7), 559–582, doi:10.1016/0011-7471(76)90001-2.

Breugem, W.-P., P. Chang, and C. Jang (2008), Barrier layers and tropical Atlantic SST biases in coupled GCMs, *Tellus, Ser. A*, *60*(5), 885–897, doi:10.1111/j.1600-0870.2008.00343.x.

Brodeau, L., B. Barnier, A.-M. Treguier, T. Penduff, and S. Gulev (2010), An ERA40-based atmospheric forcing for global ocean circulation models, *Ocean Modell.*, *31*(3–4), 88–104, doi:10.1016/j.ocemod.2009.10.005.

Caniaux, G., H. Giordani, J.-L. Redelsperger, F. Guichard, E. Key, and M. Wade (2011), Coupling between the Atlantic cold tongue and the West African monsoon in boreal spring and summer, *J. Geophys. Res.*, *116*, C04003, doi:10.1029/2010JC006570.

Da-Allada, C. Y., G. Alory, Y. du Penhoat, E. Kestenare, F. Durand, and N. M. Hounkonnou (2013), Seasonal mixed-layer salinity balance in the tropical Atlantic Ocean: Mean state and seasonal cycle, *J. Geophys. Res. Oceans*, *118*, 332–345, doi:10.1029/2012JC008357.

Da-Allada, C., Y. du Penhoat, J. Jouanno, G. Alory, and N. Hounkonnou (2014), Modeled mixed-layer salinity balance in the Gulf of Guinea: Seasonal and interannual variability, *Ocean Dyn.*, *64*(12), 1783–1802, doi:10.1007/s10236-014-0775-9.

Dai, A., and K. Trenberth (2002), Estimates of freshwater discharge from continents: Latitudinal and seasonal variations, *J. Hydrometeorol.*, *3*, 660–687.

Danabasoglu, G., et al. (2014), North Atlantic simulations in coordinated ocean-ice reference experiments phase II (core-ii). Part I: Mean states, *Ocean Modell.*, *73*, 76–107, doi:10.1016/j.ocemod.2013.10.005.

de Boyer Montégut, C., G. Madec, and A. Fischer (2004), Mixed layer depth over the global ocean: An examination of profile data and a profile-based climatology, *J. Geophys. Res.*, *109*, C12003, doi:10.1029/2004JC002378.

Dessier, A., and J. R. Donguy (1994), The sea surface salinity in the tropical Atlantic between 10°S and 30°N—Seasonal and interannual variations (1977–1989), *Deep Sea Res., Part I*, *41*, 81–100.

Ding, H., N. S. Keenlyside, and M. Latif (2009), Seasonal cycle in the upper equatorial Atlantic Ocean, *J. Geophys. Res.*, *114*, C09016, doi:10.1029/2009JC005418.

du Penhoat, Y. D., and A. M. Treguier (1985), The seasonal linear response of the tropical Atlantic Ocean, *J. Phys. Oceanogr.*, *15*, 316–329, doi:10.1175/1520-0485(1985)015<0316:TSLROT>2.0.CO;2.

Durack, P. J., S. E. Wijffels, and R. J. Matear (2012), Ocean salinities reveal strong global water cycle intensification during 1950 to 2000, *Science*, *336*(6080), 455–458, doi:10.1126/science.1212222.

Foltz, G. R., and M. J. McPhaden (2008), Seasonal mixed layer salinity balance of the tropical North Atlantic Ocean, *J. Geophys. Res.*, *113*, C02013, doi:10.1029/2007JC004178.

Foltz, G. R., and M. J. McPhaden (2009), Impact of barrier layer thickness on SST in the central Tropical North Atlantic, *J. Clim.*, *22*, 285–299, doi:10.1175/2008JCLI2308.1.

Foltz, G. R., S. A. Grodsky, J. A. Carton, and M. J. McPhaden (2004), Seasonal salt budget of the northwestern tropical Atlantic Ocean along 38°W, *J. Geophys. Res.*, *109*, C03052, doi:10.1029/2003JC002111.

Foltz, G. R., C. Schmid, and R. Lumpkin (2013), Seasonal cycle of the mixed layer heat budget in the northeastern tropical Atlantic Ocean, *J. Clim.*, *26*, 8169–8188, doi:10.1175/JCLI-D-13-00037.1.

Foltz, G. R., C. Schmid, and R. Lumpkin (2015), Transport of surface freshwater from the equatorial to the subtropical north Atlantic Ocean, *J. Phys. Oceanogr.*, *45*, 1086–1102, doi:10.1175/JPO-D-14-0189.1.

Godfrey, J. S., and E. J. Lindstrom (1989), The heat budget of the equatorial western Pacific surface mixed layer, *J. Geophys. Res.*, *94*, 8007–8017.
Gordon, A. L., and K. T. Bosley (1991), Cyclonic gyre in the tropical south Atlantic, *Deep Sea Res., Part A*, *1*, S323–S343, doi:10.1016/S0198-0149(12)80015-X.
Griffies, S. M., et al. (2009), Coordinated ocean-ice reference experiments (cores), *Ocean Modell.*, *26*(12), 1–46, doi:10.1016/j.ocemod.2008.08.007.
Griffies, S. M., et al. (2015), Impacts on ocean heat from transient mesoscale eddies in a hierarchy of climate models, *J. Clim.*, *28*, 952–977, doi:10.1175/JCLI-D-14-00353.1.
Grodsky, S. A., J. A. Carton, S. Nigam, and Y. M. Okumura (2012), Tropical Atlantic biases in CCSM4, *J. Clim.*, *25*, 3684–3701, doi:10.1175/JCLI-D-11-00315.1.
Haarsma, R., E. Campos, S. Drijfhout, W. Hazeleger, and C. Severijns (2011), Impacts of interruption of the Agulhas leakage on the tropical Atlantic in coupled ocean atmosphere simulations, *Clim. Dyn.*, *36*(5–6), 989–1003, doi:10.1007/s00382-009-0692-7.
Han, W., J. P. McCreary, and K. E. Kohler (2001), Influence of precipitation minus evaporation and Bay of Bengal rivers on dynamics, thermodynamics, and mixed layer physics in the upper Indian Ocean, *J. Geophys. Res.*, *106*(C4), 6895–6916, doi:10.1029/2000JC000403.
Handoh, I. C., and G. R. Bigg (2000), A self-sustaining climate mode in the tropical Atlantic, 1995–97: Observations and modelling, *Q. J. R. Meteorol. Soc.*, *126*(564), 807–821, doi:10.1002/qj.49712656403.
Hasson, A., T. Delcroix, and J. Boutin (2013a), Formation and variability of the South Pacific Sea surface salinity maximum in recent decades, *J. Geophys. Res. Oceans*, *118*, 5109–5116, doi:10.1002/jgrc.20367.
Hasson, A. E. A., T. Delcroix, and R. Dussin (2013b), An assessment of the mixed layer salinity budget in the tropical Pacific Ocean: Observations and modelling (1990–2009), *Ocean Dyn.*, *63*(2–3), 179–194, doi:10.1007/s10236-013-0596-2.
Hu, Z.-Z., and B. Huang (2007), Physical processes associated with the tropical Atlantic SST gradient during the anomalous evolution in the southeastern ocean, *J. Clim.*, *20*, 3366–3378, doi:10.1175/JCLI4189.1.
Hummels, R., M. Dengler, P. Brandt, and M. Schlundt (2014), Diapycnal heat flux and mixed layer heat budget within the Atlantic cold tongue, *Clim. Dyn.*, *43*(11), 3179–3199, doi:10.1007/s00382-014-2339-6.
Jackett, D. R., and T. J. McDougall (1985), An oceanographic variable for the characterization of intrusions and water masses, *Deep Sea Res., Part A*, *32*(10), 1195–1207, doi:10.1016/0198-0149(85)90003-2.
Jackett, D. R., and T. J. McDougall (1995), Minimal adjustment of hydrographic data to achieve static stability, *J. Atmos. Oceanic Technol.*, *12*, 381–389.
Jouanno, J., and J. Sheinbaum (2013), Heat balance and eddies in the Caribbean upwelling system, *J. Phys. Oceanogr.*, *43*, 1004–1014, doi:10.1175/JPO-D-12-0140.1.
Jouanno, J., F. Marin, Y. du Penhoat, J. Sheinbaum, and J.-M. Molines (2011), Seasonal heat balance in the upper 100 m of the equatorial Atlantic Ocean, *J. Geophys. Res.*, *116*, C09003, doi:10.1029/2010JC006912.
Jouanno, J., F. Marin, Y. du Penhoat, and J.-M. Molines (2012), Intraseasonal modulation of the surface cooling in the Gulf of Guinea, *J. Phys. Oceanogr.*, *43*, 382–401, doi:10.1175/JPO-D-12-053.1.
Kolodziejczyk, N., and F. Gaillard (2012), Observation of spiciness interannual variability in the pacific pycnocline, *J. Geophys. Res.*, *117*, C12018, doi:10.1029/2012JC008365.
Kolodziejczyk, N., and F. Gaillard (2013), Variability of the heat and salt budget in the subtropical southeastern pacific mixed layer between 2004 and 2010: Spice injection mechanism, *J. Phys. Oceanogr.*, *43*, 1880–1898, doi:10.1175/JPO-D-13-04.1.
Kolodziejczyk, N., B. Bourls, F. Marin, J. Grelet, and R. Chuchla (2009), Seasonal variability of the equatorial undercurrent at 10°W as inferred from recent in situ observations, *J. Geophys. Res.*, *114*, C06014, doi:10.1029/2008JC004976.
Kolodziejczyk, N., G. Reverdin, F. Gaillard, and A. Lazar (2014a), Low-frequency thermohaline variability in the subtropical south Atlantic pycnocline during 2002–2013, *Geophys. Res. Lett.*, *41*, 6468–6475, doi:10.1002/2014GL061160.
Kolodziejczyk, N., F. Marin, B. Bourls, Y. Gouriou, and H. Berger (2014b), Seasonal variability of the equatorial undercurrent termination and associated salinity maximum in the Gulf of Guinea, *Clim. Dyn.*, *43*(11), 3025–3046, doi:10.1007/s00382-014-2107-7.
Langehaug, H. R., P. B. Rhines, T. Eldevik, J. Mignot, and K. Lohmann (2012), Water mass transformation and the North Atlantic Current in three multicentury climate model simulations, *J. Geophys. Res.*, *117*, C11001, doi:10.1029/2012JC008021.
Large, W. G., G. Danabasoglu, S. C. Doney, and J. C. McWilliams (1997), Sensitivity to surface forcing and boundary layer mixing in a global ocean model: Annual-mean climatology, *J. Phys. Oceanogr.*, *27*, 2418–2447, doi:10.1175/1520-0485(1997)027<2418:STSFAB>2.0.CO;2.
Latif, M., E. Roeckner, U. Mikolajewicz, and R. Voss (2000), Tropical stabilization of the thermohaline circulation in a greenhouse warming simulation, *J. Clim.*, *13*(11), 1809–1813, doi:10.1175/1520-0442(2000)013<1809:L>2.0.CO;2.
Laurian, A., A. Lazar, G. Reverdin, K. Rodgers, and P. Terray (2006), Poleward propagation of spiciness anomalies in the North Atlantic Ocean, *Geophys. Res. Lett.*, *33*, L13603, doi:10.1029/2006GL026155.
Laurian, A., A. Lazar, and G. Reverdin (2009), Generation mechanism of spiciness anomalies: An OGCM analysis in the North Atlantic subtropical gyre, *J. Phys. Oceanogr.*, *39*(4), 1003–1018, doi:10.1175/2008JPO3896.1.
Lazar, A., R. Murtugudde, and A. J. Busalacchi (2001), A model study of temperature anomaly propagation from the subtropics to tropics within the south Atlantic thermocline, *Geophys. Res. Lett.*, *28*(7), 1271–1274, doi:10.1029/2000GL011418.
Levitus, S., T. Boyer, M. Conkright, T. O'Brien, J. Antonov, C. Stephens, L. Stathoplos, D. Johnson, and R. Gelfeld (Eds.) (1998), *World Ocean Database 1998: Introduction*, vol. 1, 346 pp., U.S. Gov. Print. Off., Washington, D. C.
Levitus, S., J. Antonov, and T. Boyer (2005), Warming of the world ocean, 1955–2003, *Geophys. Res. Lett.*, *32*, L02604, doi:10.1029/2004GL021592.
Liu, H., S. A. Grodsky, and J. A. Carton (2009), Observed sub seasonal variability of oceanic barrier and compensated layers, *J. Clim.*, *22*(22), 6104–6119, doi:10.1175/2009JCLI2974.1.
Liu, Z. (2012), Dynamics of interdecadal climate variability: A historical perspective, *J. Clim.*, *25*, 1963–1995, doi:10.1175/2011JCLI3980.1.
Lukas, R., and E. Lindstrom (1991), The mixed layer of the western equatorial Pacific Ocean, *J. Geophys. Res.*, *96*, 3343–3357.
Lumpkin, R., and S. L. Garzoli (2005), Near-surface circulation in the tropical Atlantic Ocean, *Deep Sea Res., Part I*, *52*(3), 495–518, doi:10.1016/j.dsr.2004.09.001.
Madec, G. (2008), NEMO ocean engine, *Tech. Rep. 27*, Inst. Pierre Simon Laplace, Paris, France.
Marin, F., G. Caniaux, H. Giordani, B. Bourlès, Y. Gouriou, and E. Key (2009), Why were sea surface temperatures so different in the eastern equatorial Atlantic in June 2005 and 2006?, *J. Phys. Oceanogr.*, *39*, 1416–1431, doi:10.1175/2008JPO4030.1.
Marsland, S., H. Haak, J. Jungclaus, M. Latif, and F. Rske (2003), The Max-Planck-Institute global ocean/sea ice model with orthogonal curvilinear coordinates, *Ocean Modell.*, *5*(2), 91–127, doi:10.1016/S1463-5003(02)00015-X.

Masson, S., J.-J. Luo, G. Madec, J. Vialard, D. F., S. Gualdi, E. Guilyardi, S. Behera, P. Delecluse, A. Navarra, and P. Yamagata (2005), Impact of barrier layer on winter-spring variability of the southeastern Arabian Sea, *Geophys. Res. Lett.*, *32*, L07703, doi:10.1029/2004GL021980.

Mignot, J., and C. Frankignoul (2004), Interannual to interdecadal variability of sea surface salinity in the Atlantic and its link to the atmosphere in a coupled model, *J. Geophys. Res.*, *109*, C04005, doi:10.1029/2003JC002005.

Mignot, J., C. de Boyer Montégut, A. Lazar, and S. Cravatte (2007), Control of salinity on the mixed layer depth in the world ocean: 2. Tropical areas, *J. Geophys. Res.*, *112*, C10010, doi:10.1029/2006JC003954.

Mignot, J., C. de Boyer Montégut, and M. Tomczak (2009), On the porosity of barrier layers, *Ocean Sci.*, *5*, 379–387, doi:10.5194/os-5-379-2009.

Mignot, J., A. Lazar, and M. Lacarra (2012), On the formation of barrier layers and associated vertical temperature inversions: A focus on the northwestern tropical Atlantic, *J. Geophys. Res.*, *117*, C02010, doi:10.1029/2011JC007435.

Mitchell, T. P., and J. M. Wallace (1992), The annual cycle in equatorial convection and sea surface temperature, *J. Clim.*, *5*, 1140–1156, doi:10.1175/1520-0442(1992)005<1140:TACIEC>2.0.CO;2.

Molines, J. M., B. Barnier, T. Penduff, L. Brodeau, A. M. Treguier, S. Theetten, and G. Madec (2007), Definition of the interannual experiment orca025-g70, 1958–2004, Technical report, LEGI-DRA-2-11-2006i, Lab. des Ecoulements Geophys. et Ind., Grenoble, France.

Muller-Karger, F. E., C. R. McClain, and P. L. Richardson (1988), The dispersal of the Amazon water, *Nature*, *333*, 56–59, doi:10.1038/333056a0.

Peter, A.-C., M. Le Hnaff, Y. du Penhoat, C. E. Menkes, F. Marin, J. Vialard, G. Caniaux, and A. Lazar (2006), A model study of the seasonal mixed layer heat budget in the equatorial Atlantic, *J. Geophys. Res.*, *111*, C06014, doi:10.1029/2005JC003157.

Philander, S. G. H., and R. C. Pacanowski (1986), A model of the seasonal cycle in the tropical Atlantic Ocean, *J. Geophys. Res.*, *91*(C12), 14,192–14,206, doi:10.1029/JC091iC12p14192.

Qu, T., S. Gao, and I. Fukumori (2011), What governs the North Atlantic salinity maximum in a global GCM?, *Geophys. Res. Lett.*, *38*, L07602, doi:10.1029/2011GL046757.

Qu, T., S. Gao, and I. Fukumori (2013), Formation of salinity maximum water and its contribution to the overturning circulation in the North Atlantic as revealed by a global general circulation model, *J. Geophys. Res. Oceans*, *118*, 1982–1994, doi:10.1002/jgrc.20152.

Reverdin, G., E. Kestenare, C. Frankignoul, and T. Delcroix (1997), Surface salinity in the Atlantic Ocean (30°S50°N), *Prog. Oceanogr.*, *73*, 311–340, doi:10.1016/j.pocean.2006.11.004.

Richardson, P. L., and T. K. McKee (1984), Average seasonal variation of the Atlantic Equatorial Currents from historical ship drifts, *J. Phys. Oceanogr.*, *14*, 1226–1238, doi:10.1175/1520-0485(1984)014<1226:ASVOTA>2.0.CO;2.

Roullet, G., and G. Madec (2000), Salt conservation, free surface, and varying levels: A new formulation for ocean general circulation models, *J. Geophys. Res.*, *105*(C10), 23,927–23,942, doi:10.1029/2000JC900089.

Sasaki, Y. N., N. Schneider, N. Maximenko, and K. Lebedev (2010), Observational evidence for propagation of decadal spiciness anomalies in the North Pacific, *Geophys. Res. Lett.*, *37*, L07708, doi:10.1029/2010GL042716.

Schneider, N. (2000), A decadal spiciness mode in the tropics, *Geophys. Res. Lett.*, *27*(2), 257–260, doi:10.1029/1999GL002348.

Terray, L., L. Corre, S. Cravatte, T. Delcroix, G. Reverdin, and A. Ribes (2012), Near-surface salinity as natures rain gauge to detect human influence on the tropical water cycle, *J. Clim.*, *25*, 958–977, doi:10.1175/JCLI-D-10-05025.1.

Thierry, V., A.-M. Treguier, and H. Mercier (2004), Numerical study of the annual and semi-annual fluctuations in the deep equatorial Atlantic Ocean, *Ocean Modell.*, *6*(1), 1–30, doi:10.1016/S1463–5003(02)00054-9.

Trenberth, K. E., and C. J. Guillemot (1998), Evaluation of the atmospheric moisture and hydrological cycle in the NCEP/NCAR reanalyses, *Clim. Dyn.*, *14*(3), 213–231, doi:10.1007/s003820050219.

Trenberth, K. E., J. M. Caron, and D. P. Stepaniak (2001), The atmospheric energy budget and implications for surface fluxes and ocean heat transports, *Clim. Dyn.*, *17*(4), 259–276, doi:10.1007/PL00007927.

Tzortzi, E., S. A. Josey, M. Srokosz, and C. Gommenginger (2013), Tropical Atlantic salinity variability: New insights from SMOS, *Geophys. Res. Lett.*, *40*, 2143–2147, doi:10.1002/grl.50225.

Vellinga, M., and P. Wu (2004), Low latitude freshwater influence on centennial variability of the Atlantic thermohaline circulation, *J. Clim.*, *17*(23), 4498–4511.

Vialard, J., and P. Delecluse (1998), An OGCM study for the TOGA decade. Part I: Role of salinity in the physics of the Western Pacific Fresh Pool, *J. Phys. Oceanogr.*, *28*, 1071–1088, doi:10.1175/1520-0485(1998)028<1071:AOSFTT>2.0.CO;2.

Vic, C., H. Berger, A.-M. Trguier, and X. Couvelard (2013), Dynamics of an equatorial river plume: Theory and numerical experiments applied to the Congo plume case, *J. Phys. Oceanogr.*, *44*, 980–994, doi:10.1175/JPO-D-13-0132.1.

Vinogradova, N. T., and R. M. Ponte (2013), Clarifying the link between surface salinity and freshwater fluxes on monthly to interannual time scales, *J. Geophys. Res. Oceans*, *118*, 3190–3201, doi:10.1002/jgrc.20200.

Wade, M., G. Caniaux, and Y. du Penhoat (2011), Variability of the mixed layer heat budget in the eastern equatorial Atlantic during 2005–2007 as inferred using Argo floats, *J. Geophys. Res.*, *116*, C08006, doi:10.1029/2010JC006683.

Yang, J., and T. M. Joyce (2006), Local and equatorial forcing of seasonal variations of the north equatorial countercurrent in the Atlantic Ocean, *J. Phys. Oceanogr.*, *36*, 238–254, doi:10.1175/JPO2848.1.

Yeager, S. G., and W. G. Large (2007), Observational evidence of winter spice injection, *J. Phys. Oceanogr.*, *37*, 2895–2919, doi:10.1175/2007JPO3629.1.

Yu, L. (2011), A global relationship between the ocean water cycle and near-surface salinity, *J. Geophys. Res.*, *116*, C10025, doi:10.1029/2010JC006937.